Volume 22
Number 34
14 September 2024
Pages 6851-7062

Organic & Biomolecular Chemistry

rsc.li/obc

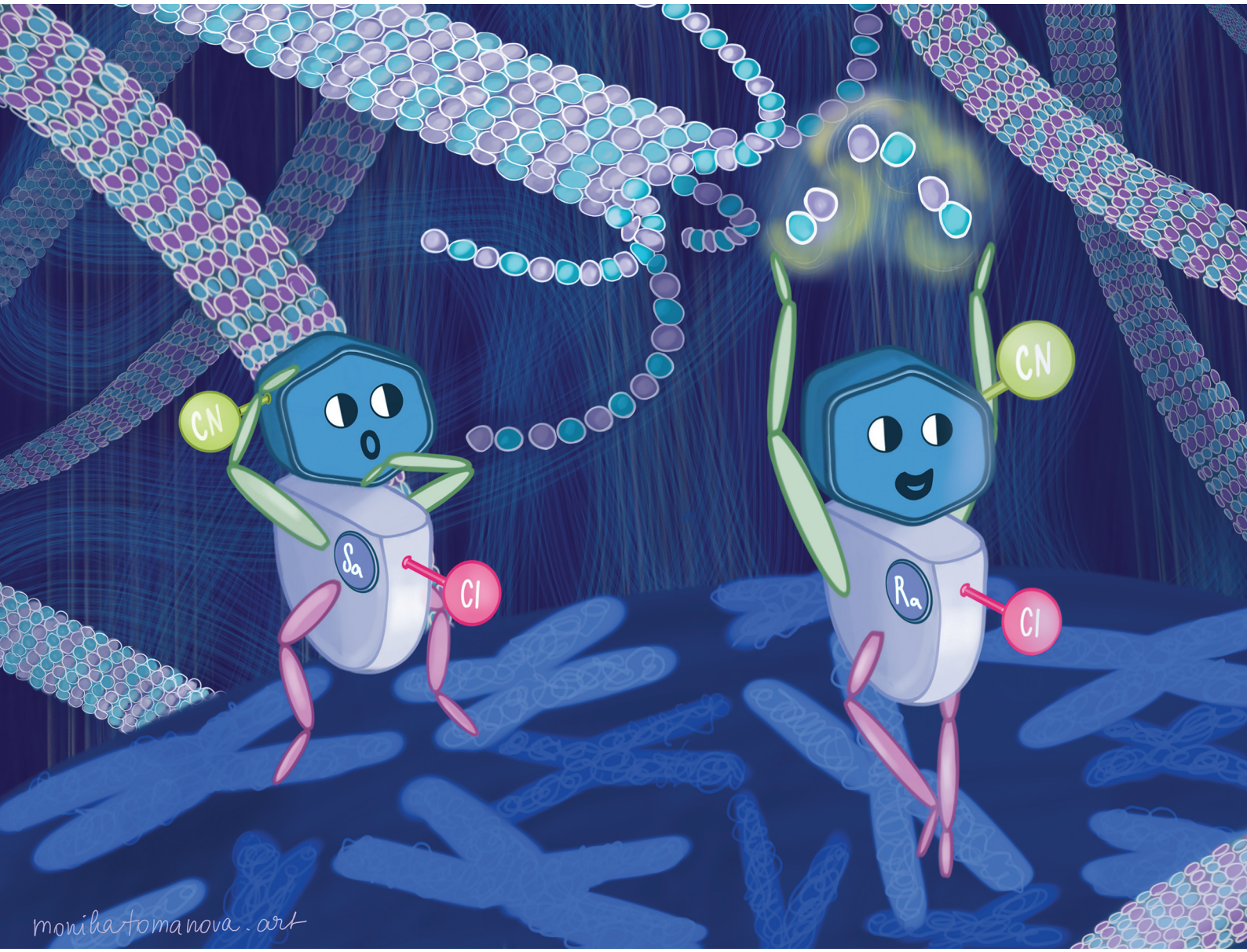

ISSN 1477-0520

ROYAL SOCIETY OF CHEMISTRY

PAPER
Lucie Rárová, Petr Cankař *et al.*
Atropisomeric 1-phenylbenzimidazoles affecting microtubule organization: influence of axial chirality

Organic & Biomolecular Chemistry

ROYAL SOCIETY OF CHEMISTRY

PAPER

View Article Online
View Journal | View Issue

Cite this: *Org. Biomol. Chem.*, 2024, **22**, 6966

Atropisomeric 1-phenylbenzimidazoles affecting microtubule organization: influence of axial chirality†

Jana Pospíšilová,[a] Tomáš Heger,[b] Ondřej Kurka,[c] Marie Kvasnicová,[b,d] Anna Chládková,[a] Ivan Nemec,[e] Lucie Rárová *[b,d] and Petr Cankař *[a]

Received 23rd May 2024,
Accepted 3rd July 2024

DOI: 10.1039/d4ob00863d

rsc.li/obc

Benzimidazoles are frequently used in medicinal chemistry. Their anticancer effect is among the most prominent biological activities exhibited by this scaffold. Although numerous benzimidazole derivatives have been synthesized, possible atropisomerism of *ortho*-substituted 1-phenylbenzimidazoles has been largely overlooked. The aim of this research was to synthesize a small library of novel atropisomeric benzimidazole derivatives and explore their biological activity in various cancer and normal human cell lines. The new unique structural motif provides an interesting 3D architecture with axial chirality, which further contributes to molecular complexity and specificity. Racemates and their separated atropisomers arrested the cell cycle, caused apoptosis, and affected microtubule organization in cancer cells *in vitro* at different intensities. Moreover, this phenomenon was also verified by the inhibition of endothelial cell migration. These results showed that (+)-atropisomers, especially **5n**, exhibit a stronger effect and show promise as agents for cancer therapy.

Introduction

For the last few decades, research in medicinal chemistry has focused on apoptosis as a method to effectively eliminate cancer cells. Tumors are defined by deregulated cell cycles that can result in loss of cellular differentiation and uncontrolled cellular growth.[1] Antiproliferative activities with different mechanisms of action including induction of apoptosis, cell cycle (G_2/M) arrest, DNA alkylation, disruption of tubulin polymerization, enzyme inhibition, antiangiogenic effects, and blockage of glucose transport can be affected by inhibitors based on benzimidazoles.[2,3] Nocodazole, galeterone, pracinostat, dovitinib, liarozole, abemaciclib, veliparib, glasdegib, selumetinib, bendamustine, and crenolanib are used to treat various malignancies[4] (Fig. 1).

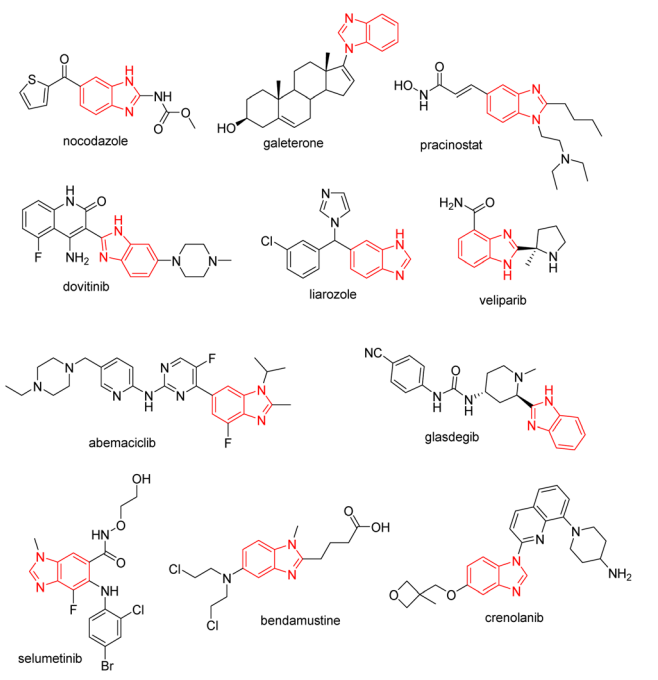

Fig. 1 Benzimidazole scaffolds in anticancer drugs.

[a]*Department of Organic Chemistry, Faculty of Science, Palacký University Olomouc, 17. listopadu 1192/12, 77900 Olomouc, Czech Republic.*
E-mail: petr.cankar@upol.cz
[b]*Department of Experimental Biology, Faculty of Science, Palacký University Olomouc, Slechtitelu 27, 77900 Olomouc, Czech Republic.*
E-mail: lucie.rarova@upol.cz
[c]*Laboratory of Growth Regulators, Institute of Experimental Botany of the Czech Academy of Sciences, and Faculty of Science, Palacký University, Slechtitelu 27, Olomouc CZ-77900, Czech Republic*
[d]*Laboratory of Growth Regulators, Institute of Experimental Botany of the Czech Academy of Science, Palacký University, Slechtitelu 27, 77900 Olomouc, Czech Republic*
[e]*Department of Inorganic Chemistry, Faculty of Science, Palacký University Olomouc, 17. listopadu 1192/12, 77900 Olomouc, Czech Republic*

†Electronic supplementary information (ESI) available. CCDC 2285266 and 2285267. For ESI and crystallographic data in CIF or other electronic format see DOI: https://doi.org/10.1039/d4ob00863d

Furthermore, aminobenzimidazoles were reported as p38α MAP kinase inhibitors[5] or compounds targeting angiogenesis to impact the migration of endothelial cells.[6] 1-Aryl substituted benzimidazoles are also promising molecules for cancer treatment. Previous publications reported that CCL299 exhibits anticancer activity through apoptosis,[7] and two older extensive SAR studies demonstrated 1-phenylbenzimidazoles as selective ATP site inhibitors.[8,9] Another aryl substitution at position 2 provides also anticancer activity as a p38 kinase inhibitor,[10] and moreover, other interesting activities, such as antimicrobial agents,[11] COX-1 and COX-2 inhibitors,[12,13] or hTRPV-1 antagonists,[14] were described.

Currently, multidrug resistance in the treatment of cancer is increasing, which strengthens the need to develop novel chemotherapeutics based on benzimidazoles.[1] As shown in Fig. 1, the benzimidazole scaffold can be variously substituted to obtain different structural patterns with modified anticancer activity. The structural motif, in which benzimidazole is substituted with two adjacent aryls at positions 1 and 2, was also studied.[15–19] However, the substitution at these aryls was always designed to avoid atropisomerism since the stability of these atropisomers can be insufficient.[20] For this reason, the aryls were usually designed to be symmetrical or not *ortho*-substituted. The possibility of introducing axial chirality to similar derivatives inspired us to study the impact on the cytotoxicity of benzimidazoles since this phenomenon has been poorly covered in the literature despite its importance and prevalence.

Our ongoing research is oriented towards axially chiral benzimidazoles[21–24] because atropisomerism of these compounds provides an interesting three-dimensional (3D) structure, which can further enrich the chemical space in the area of benzimidazole derivatives. In this study, we focused our attention on 1-phenylbenzimidazoles, in which the *ortho*-substituents at the benzene ring restricts the free rotation around the single C–N bond at position 1 to generate axial chirality (Fig. 2). To obtain stable atropisomers, we chose substituents that could generate a high energy barrier and eliminate possible racemization.

Although similar compounds have been reported as sirtuin inhibitors[16,18] or anti-tubulin polymerization agents,[15,17] the biological issues associated with the presence of axial chirality remained unexamined for this class of compounds. Our goal was to find novel axially chiral benzimidazole-based agents with potential antiproliferative or antiangiogenic activities. The objectives of our research were to (i) synthesize novel unique axially chiral benzimidazoles, (ii) investigate their biological activities in cancer cells *in vitro* (cytotoxicity and antiproliferative activity), (iii) induct cancer cell apoptosis and determine its mechanism of action, and (iv) separate the most interesting compounds to single atropisomers and explore their biological activity and stability.

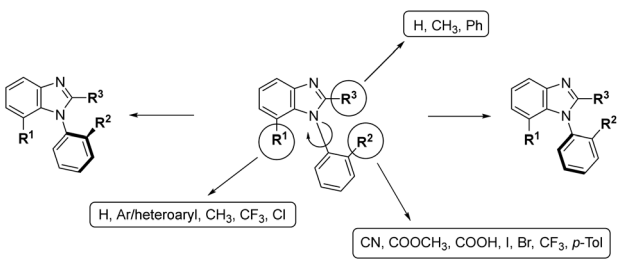

Fig. 2 Atropisomerism of 1-phenylbenzimidazoles due to the restricted rotation around the single C–N bond.

Results and discussion

Chemistry

Benzimidazoles were effectively synthesized in several steps (Scheme 1). The first step was nucleophilic aromatic substitution of various fluoronitrobenzenes with *o*-substituted anilines using KOH in DMSO to obtain nitroanilines **3a–j** in very good yields. The most convenient route to synthesize the final benzimidazoles was reducing the nitro group with catalytic hydrogenation in acetic acid (**4a**) or with zinc in a solution of methanol and acetic acid (**4b–f**), followed by cyclization with orthoesters to obtain compounds **5a–o**. Moreover, we synthesized compounds **5a–f** and **8a–b** from intermediates after aromatic nucleophilic substitution or Suzuki–Miyaura coupling in just two steps by one-pot reduction and cyclization with trimethyl orthoformate. Compounds **3a** and **3e** can be modified by Suzuki–Miyaura cross-coupling with various aryl/heteroaryl boronic acids to form **6a–e** or **9**. Precatalyst XPhos Pd G2 was used to provide excellent yields.[25,26] Reduction of the nitro group led to phenylenediamines **7a–f** and **10**, and an

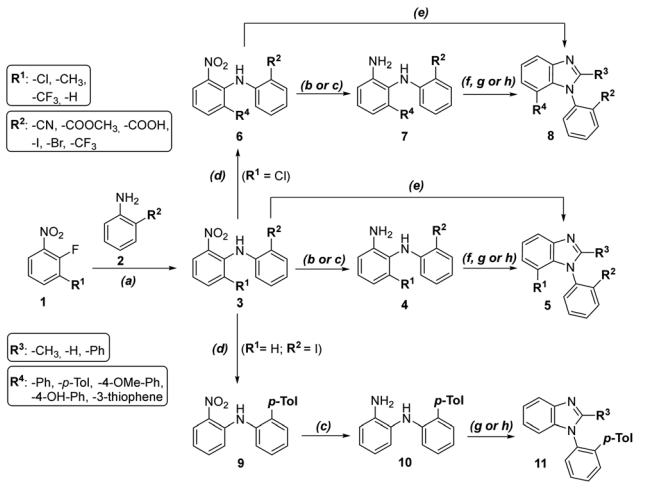

Scheme 1 General synthetic scheme. Reagents and conditions: (a) KOH, DMSO, rt, 4–12 h, 47–88%; (b) H_2, Pd/C, AcOH, rt, 1.5 h, 73–88%; (c) Zn, MeOH : AcOH 4 : 1, rt, 10–60 min, 48–74%; (d) aryl/heteroarylboronic acid, K_3PO_4, XPhos Pd G2, dioxane : water 4 : 1, 100 °C, 2.5 h, 35–97%; (e) Zn, MeOH : AcOH 4 : 1, rt, 10–60 min, then trimethyl orthoformate, rt, overnight, 49–87%; (f) trimethyl orthoformate, *p*TSA, DCM, rt, overnight, 16–80%; (g) trimethyl orthoacetate, *p*TSA, DCM, rt, overnight, 44–81%; (h) trimethyl orthobenzoate, *p*TSA, DCM, rt, overnight, 40–75%.

analogous cyclization protocol generated benzimidazoles **8c–l** and **11a–b** for the SAR study.

Biology

Cytotoxicity in cancer and normal cells. The series of 29 novel benzimidazole derivatives was tested in seven cancer cell lines of various histopathological origin and two normal cells to compare cytotoxicity in normal cells *in vitro* after 72 h. Most of the tested compounds exhibited moderate cytotoxic activity. The three most interesting compounds (**5l**, **5m**, and **5n**) showed strong cytotoxic activity toward cancer cells (A2780, G-361, HeLa, and MV4-11) and no cytotoxicity toward at least one normal cell type (RPE-1 or BJ) (Table 1). The *ortho*-substitution (R^2) with carboxyl or ester functionality (**5e** and **5h**) practically eliminated the cytotoxic effect. The essentiality of the *ortho*-substitution confirmed the difference in cytotoxicity between **5n** and **5o**. We chose the seven most active compounds from the first screening and we tested them in an additional five cancer cell lines (A172, K562, LNCaP, and THP-1). The three most interesting substances were again **5l**, **5m**, and **5n** (Table S3†).

Generally, we observed interesting trends for the SAR study. Among the compounds, those with iodine as the R^2 substituent provided the best biological properties, and these compounds are not toxic toward normal cells. Benzimidazole **5n** with nitrile (R^2), phenyl (R^3), and chlorine (R^1) provided the best biological activity in cancer cells (especially HeLa = 3.2 μM, G-361 = 4.4 μM); however, while the compound was not toxic to BJ cells, it was toxic to normal RPE-1 cells (23.4 μM). Changing nitrile to iodine in derivative **5l** led to very interesting biological activity against cancer cell lines (HeLa = 9.3 μM, G-361 = 9.8 μM) and no activity toward normal cells.

As the essentiality of atropisomerism for cytotoxicity was indirectly illustrated by the synthesis of non *ortho*-substituted benzimidazole **5o**, we also decided to study separated atropisomers of the most active benzimidazoles **5l** and **5n**, which further enrich the 3D structure with axial chirality.

Stability and biological activity of separated atropisomers. The most active compounds **5l** and **5n** were chosen for additional experiments and separated into individual atropisomers by chiral semipreparative HPLC (Fig. 3). The absolute configuration was determined by the X-ray single-crystal diffraction method. Both (+)-atropisomers were revealed to have an absolute configuration (R_a). The atropisomers were heated in ethylene glycol to test their stabilities, and racemization was monitored by chiral HPLC. **(+)-5l** remained stable at 100 °C for 24 h, which indicates very good stability (ΔE_{rot} >30 kcal mol^{-1}). **(−)-5n** started racemizing at 100 °C, where we obtained 6% of the opposite atropisomer after 15 min (88% ee), and racemization was almost complete after 5 h (see ESI†).

We compared the cytotoxicity of racemates and single atropisomers in six cancer and two normal cell lines (Table 2). These cell lines were selected as the most interesting according to the IC_{50}s values of **5l** and **5n** from Tables 1 and 2. Racemic **5l** and **5n** and separated enantiopure atropisomers were cytotoxic toward cancer cell lines (A2780, CEM, G-361, HeLa, MCF7, and MV4-11), but not toward normal skin cells (BJ) for 72 h. The most sensitive cell lines toward our racemic **5l** and **5n** and single enantiopure atropisomers were B-myelomonocytic leukemia MV4-11, cervical carcinoma HeLa, and malignant melanoma G-361, with activities fluctuating around similar levels. Benzimidazole **5n** showed significant differences in activities between single atropisomers for all six measured cancer lines and iodo derivative **5l** for HeLa, G-361, and A2780 cells. Moreover, in MV4-11 cells, the cytotoxicity of **(+)-5n** was 7.5 × higher than that of its (−)-atropisomer (Table 2). The IC_{50}s values for racemates are slightly different from the results in Table 1 because other biological replicates were used, which were performed in one set with atropisomers. Experiments were repeated three times with three technical replicates.

Antiproliferative activity in cancer cells. The activity of the compounds differed in selectivity against noncancerous and cancerous cells, as shown in the cytotoxicity screening. MV4-11 and HeLa cells were chosen for further experiments because they exhibited the lowest IC_{50}s values toward **5l** and **5n** and interesting selectivity between the activity of racemates and their atropisomers. As mentioned above, MV4-11 cells were much more sensitive towards **(+)-5n** than **(−)-5n**.

The influence of racemates **5l** and **5n** along with purified atropisomers on the MV4-11 and HeLa cells after 24 h of treatment was compared in a series of experiments, including immunoblotting, cell cycle analysis, and/or immunofluorescence and caspase-3/7 activity assays. Protein extracts from cells treated with 15 μM compounds for 24 h were analyzed by SDS-PAGE followed by immunoblotting. Induction of apoptosis in MV4-11 and HeLa cells with 15 μM racemates and (+)-atropisomers **5l** and **5n** was detected after 24 h of treatment (Fig. 4). As a marker of apoptosis, the caspase-7 fragment was specifically found in the compound-treated cells but not in the DMSO control samples. The lowest band intensity was observed in the sample treated with atropisomer **(–)-5n**, whereas **(+)-5n** provided the densest band among benzimidazole compounds. The cleavage of caspase-7 substrate, poly (ADP-ribose) polymerase PARP, was found in the same treatments by racemates and (+)-atropisomers as caspase-7 fragment was observed. In addition, the marker of mitosis, p-histone H3 at Ser 10 [27] was also induced by racemates and (+)-atropisomers (Fig. 4A and B). This induction of p-histone H3 indicated G_2/M arrest. The most active compounds were racemates and **(+)-5l** and **(+)-5n**.

In MV4-11 cells stained with propidium iodide and analyzed for the DNA content by a flow cytometry, apoptotic events appeared as the sub-G1 (debris) fraction increased. In the samples treated with 15 μM compounds for 24 h, the elevated sub-G1 fraction correlated with both the caspase activity measurements and immunoblotting. The overall difference between atropisomers regarding their influence on the cell cycle was more pronounced in **5n** than in **5l**. The sub-G1 cell population rose rapidly along with the G2/M block observed in the treatments with higher concentrations of compounds. This effect was observed from 7.5 μM **(+)-5n** to higher concen-

Table 1 Cytotoxicity presented as IC_{50} (μM) in various cell lines after 72 h

	R^1/R^4	R^2	R^3	CCRF-CEM	MV4-11	MOLM-13	MCF7	HeLa	G-361	A2780	RPE-1	BJ
5a	$-CH_3$	–I	–H	40.6 ± 0.0	27.5 ± 0.8	31.9 ± 4.0	>100	28.0 ± 3.3	23.3 ± 3.4	25.5 ± 4.6	>100	—
5b	–Cl	$-CF_3$	–H	31.2 ± 2.4	14.5 ± 1.5	16.2 ± 0.1	14.2 ± 0.3	22.5 ± 4.2	59.8 ± 4.5	16.3 ± 2.2	>100	—
5c	–Cl	–I	–H	42.0 ± 1.3	20.5 ± 2.2	28.3 ± 0.1	26.9 ± 2.4	18.0 ± 0.1	69.9 ± 1.5	18.6 ± 2.5	>100	—
5d	$-CF_3$	–I	–H	60.0 ± 7.0	29.2 ± 8.7	23.8 ± 7.7	41.8 ± 5.4	22.8 ± 2.5	59.5 ± 0.5	20.8 ± 5.1	>100	>100
5e	–Cl	$-COOCH_3$	–H	>100	>100	>100	>100	>100	>100	71.5 ± 5.5	>100	—
5f	–Cl	–Br	–H	24.1 ± 4.5	12.3 ± 0.2	15.8 ± 1.3	14.0 ± 0.4	15.7 ± 3.2	82.6 ± 1.1	13.7 ± 1.6	>100	—
5g	–Cl	–CN	–H	>100	66.4 ± 14.7	70.9 ± 37.0	54.6 ± 10.4	42.8 ± 1.0	>100	70.6 ± 1.3	>100	—
5h	–H	–COOH	$-CH_3$	>100	>100	>100	>100	>100	>100	>100	>100	—
5i	–Cl	–I	$-CH_3$	37.7 ± 3.0	19.2 ± 2.5	27.3 ± 0.1	29.3 ± 8.3	17.1 ± 0.6	58.6 ± 4.7	18.5 ± 2.6	>100	—
5j	–H	–I	$-CH_3$	89.4 ± 3.8	54.9 ± 4.2	88.4 ± 0.2	>100	>100	>100	70.3 ± 7.4	>100	>100
5k	–Cl	–CN	$-CH_3$	>100	60.7 ± 3.8	81.2 ± 5.9	90.7 ± 7.6	56.8 ± 12.8	>100	52.2 ± 4.2	>100	—
5l	–Cl	–I	–Ph	22.9 ± 3.3	13.3 ± 4.8	11.7 ± 0.8	33.1 ± 2.4	9.3 ± 2.2	9.8 ± 0.9	13.4 ± 0.1	>100	>100
5m	$-CF_3$	–I	–Ph	17.2 ± 0.7	9.9 ± 0.8	10.0 ± 2.4	19.0 ± 5.8	11.4 ± 2.7	22.3 ± 6.9	8.6 ± 0.9	>100	—
5n	–Cl	–CN	–Ph	12.4 ± 2.1	7.8 ± 1.0	13.2 ± 1.1	15.6 ± 1.5	3.2 ± 0.5	4.4 ± 0.3	8.4 ± 1.8	23.4 ± 0.6	>50
5o	–Cl	–H	–Ph	—	—	—	>100	>100	>100	>100	>100	—
8a	–*p*Tol	–CN	–H	>100	43.7 ± 1.0	80.9 ± 17.6	>100	71.3 ± 3.5	>100	38.6 ± 10.4	>100	—
8b	–4-OH-Ph	–CN	–H	75.0 ± 2.2	39.4 ± 1.3	46.8 ± 11.7	70.9 ± 0.2	74.4 ± 2.3	96.5 ± 1.9	42.3 ± 7.7	>100	—
8c	$-4-OCH_3$-Ph	–CN	–H	>100	>100	>100	>100	>100	>100	67.0 ± 6.4	>100	—
8d	–3-thiophene	–CN	–H	>50	—	—	—	43.2 ± 0.8	—	—	—	>50
8e	–Ph	–CN	–H	>100	>100	>100	>100	>100	>100	87.5 ± 12.0	>100	—
8f	–*p*Tol	–CN	$-CH_3$	>100	>100	>100	>100	>100	>100	>100	>100	—
8g	$-4-OCH_3$-Ph	–CN	$-CH_3$	>50	—	—	—	>50	—	—	—	>50
8h	–3-thiophene	–CN	$-CH_3$	>50	—	—	—	>50	—	—	—	>50
8i	–Ph	–CN	$-CH_3$	>100	>100	>100	>100	>100	>100	74.0 ± 18.5	>100	>100
8j	$-4-OCH_3$-Ph	–CN	–Ph	>50	—	—	—	>50	—	—	—	>50
8k	–3-thiophene	–CN	–Ph	32.2 ± 3.3	—	—	—	>50	—	—	—	>50
8l	–Ph	–CN	–Ph	>50	—	—	85.5	>100	>100	22.1	>100	>50
11a	–H	–*p*Tol	$-CH_3$	>100	93.6 ± 5.9	92.8 ± 3.7	>100	>100	>100	77.0 ± 12.1	>100	—
11b	–H	–*p*Tol	–Ph	44.5 ± 3.4	36.7 ± 0.2	25.3 ± 2.8	41.7 ± 0.3	13.6 ± 1.5	15.1 ± 4.8	35.4 ± 4.0	25.3 ± 4.5	—

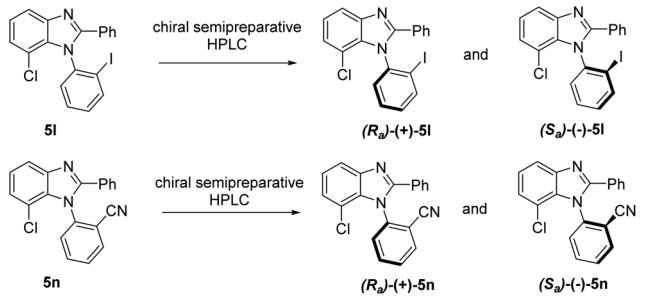

Fig. 3 Separation of **5l** and **5n** into individual atropisomers (for X-ray structures and HPLC methods see ESI†).

trations; however, this was not observed for (–)-**5n**, in which the G1 phase increased with the compound concentration.

Additionally, the sub-G1 fraction was almost not elevated in (–)-**5n**-treated samples. Similarly, (+)-**5l** appeared to be the most effective, whereas (–)-**5l** was the least effective in increasing the sub-G1 population, which probably occured *via* apoptosis. The S phase cells became more abundant in higher concentrations of the racemic mixture **5l** and the atropisomer (+)-**5l**. However, the effect diminished after the cells started to die and was not observed for (–)-**5l**. Additionally, **5n** and its atropisomers did not show this activity (Fig. 5).

In addition, the G_2/M block caused by **5n** and (+)-**5n** after 24 h is comparable to the cell cycle (G_2/M) arrest, induction of apoptosis, and disruption of microtubule polymerization by arylpyrazole-linked benzimidazole conjugates[28] and the anti-tubulin agents paclitaxel (PTX) or colchicine.[29]

In the caspase-3/7 assay, the proteolytic activity of both effector caspases is monitored by the release of a fluorescent product from a synthetic peptide substrate. The MV4-11 cells were treated with the 15 μM solutions of **5l**, **5n**, and their atropisomers for 24 h and lysed, and the lysates were mixed with the caspase-3/7 substrate. After 2 h of the substrate cleavage reaction, the fluorescence was recorded and normalized to a DMSO-treated sample to calculate the fold increase in the caspase-3/7 activity.

The activity in (–)-**5l** and (–)-**5n**-treated cells increased by 2.8- and 2.0-fold, respectively (Fig. 5). These results correlated with the cleaved caspase-7 fragment detected by immunoblot-

Table 2 Activity of racemates and separated atropisomers (IC_{50}; μM; 72 h)

	R^1	R^2	R^3	CCRF-CEM	MV4-11	MCF7	HeLa	G-361	A2780	RPE-1	BJ
5l	–Cl	–I	–Ph	22.9 ± 3.3	8.4 ± 1.1	33.1 ± 2.4	7.3 ± 0.6	5.8 ± 2.5	17.1 ± 3.8	>50	44.9 ± 0.4
(–)-**5l**	–Cl	–I	–Ph	17.8 ± 3.4	7.4 ± 0.7	16.4 ± 4.0	6.2 ± 0.1	5.0 ± 0.2	>50	>50	>50
(+)-**5l**	–Cl	–I	–Ph	12.8 ± 4.3	7.2 ± 0.4	16.0 ± 1.7	7.4 ± 0.2	8.6 ± 1.1	18.3 ± 5.0	>50	>50
5n	–Cl	–CN	–Ph	12.4 ± 2.1	8.0 ± 1.0	15.6 ± 1.5	5.1 ± 1.0	4.9 ± 0.6	15.5 ± 2.3	23.4 ± 0.6	>50
(–)-**5n**	–Cl	–CN	–Ph	18.1 ± 1.9	30.7 ± 1.3	24.0 ± 2.1	3.2 ± 1.0	2.5 ± 0.2	7.0 ± 0.3	10.5 ± 1.1	>50
(+)-**5n**	–Cl	–CN	–Ph	8.2 ± 0.5	4.1 ± 1.4	9.3 ± 1.7	4.9 ± 0.7	6.6 ± 1.1	11.3 ± 1.9	17.3 ± 0.3	>50

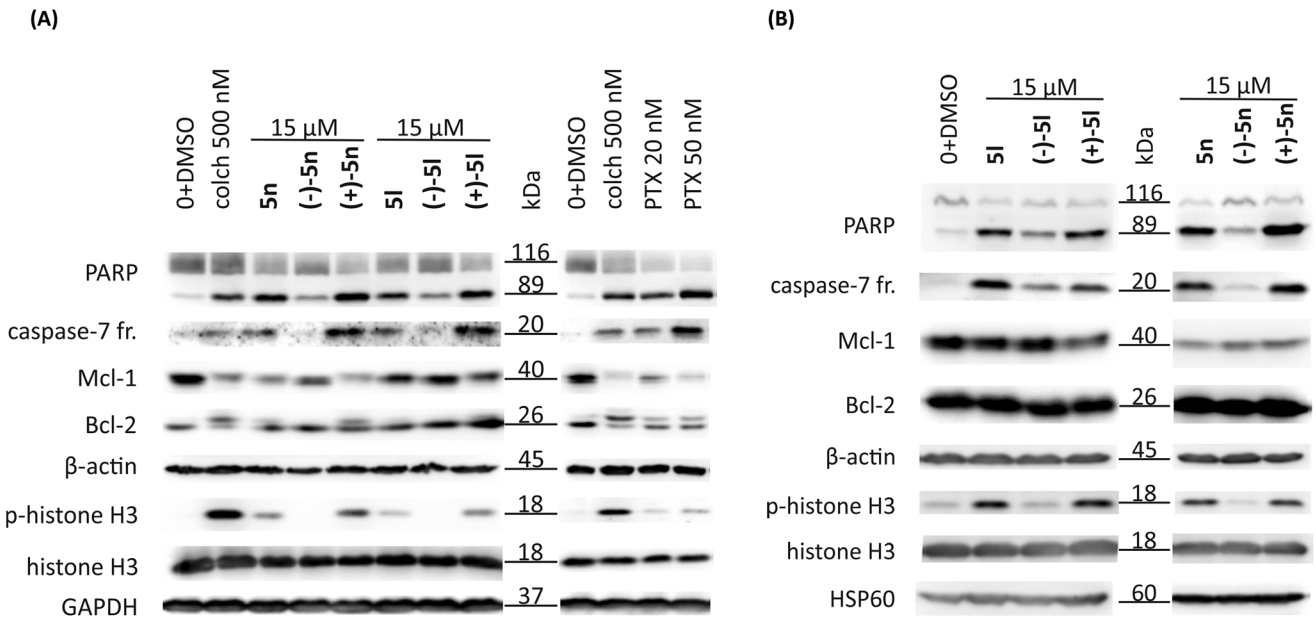

Fig. 4 Induction of apoptosis detected by western blotting. HeLa cells (A) and MV4-11 (B) were treated for 24 h with 15 μM **5l** and **5n** and their atropisomers. β-Actin and HSP60 or GAPDH were used as loading controls. p-Histone H3 was detected by an antibody recognizing phosphorylation at Ser10. 0 + DMSO are control untreated cells with DMSO at the same level as in the treatment. The results presented here are based on a representative experiment that was repeated three times. Colchicine (colch) and paclitaxel (PTX) were used as positive controls.

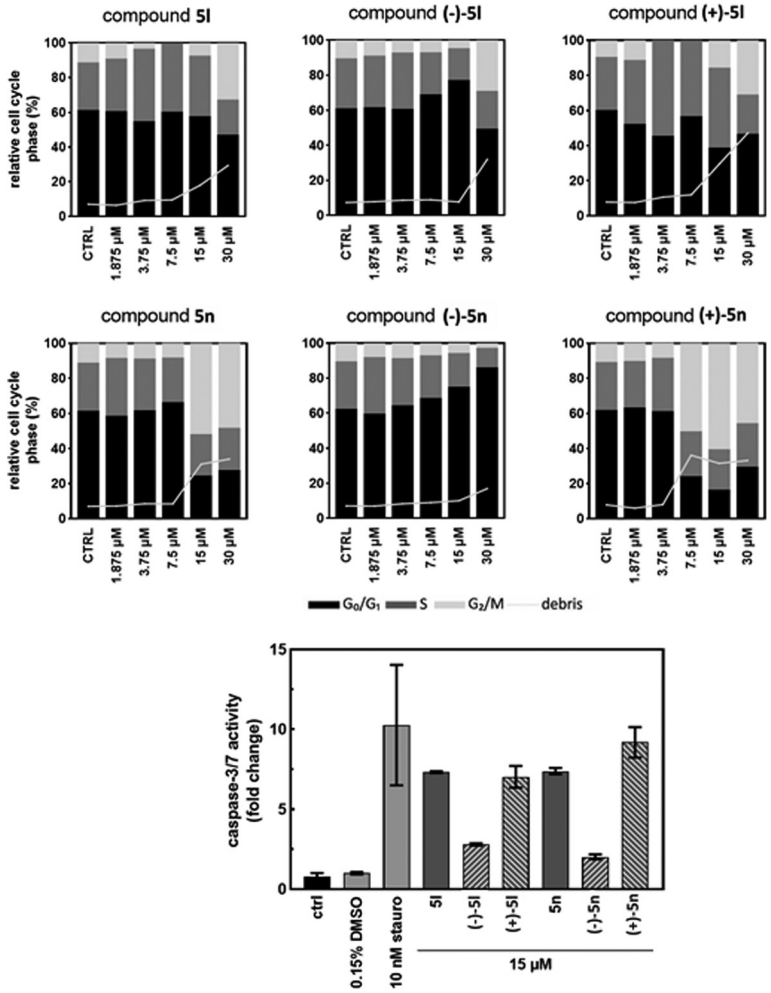

Fig. 5 Changes in the cell cycle detected by flow cytometry and caspase activity assay. MV4-11 cells were treated for 24 h with 1.875, 3.75, 7.5, 15, and 30 μM solutions of **5l** and **5n** and their atropisomers. The ctrl bars are control untreated cells, and the 0.15% DMSO bars are control cells with DMSO at the same level as in the treatment. Staurosporine (stauro) was used as the positive control. The results presented here are based on a representative experiment that was repeated three times.

ting. Opposite atropisomers, (+)-**5l** and (+)-**5n**, as well as racemic mixtures, induced a stronger response in caspase activation. The caspase-3/7 assay results were in agreement with the western blotting experiment, and both showed a clear difference in the activities of atropisomers. This demonstrates the importance of compound atropisomerism for biological activity. In the propidium iodide flow cytometry experiment, the increase in dead cells was expected, as caspase-3/7 activation is associated with the mitochondrial outer membrane permeabilization and subsequent apoptosis.[30] For the most active atropisomers (+)-**5l** and (+)-**5n**, caspase-3/7 reached 7- and 9-fold activation, respectively. Whether the activation of the caspase cascade is the main mechanism of compound cytotoxicity and what triggers these events should be investigated in further research.

(+)-Atropisomers affected the cell cycle and microtubule organization. Using flow cytometry, western blotting and immunofluorescence analysis, we tested whether racemic **5l** and **5n** and their single atropisomers can influence the cell cycle and the cytoskeleton of HeLa human cervical cancer cells, as published earlier for novel microtubule inhibitors[31–33] and paclitaxel-based microtubule stabilizers.[34] The strongest cytotoxicities of our racemates and atropisomers were measured in two adherent cancer cell lines, HeLa and G-361. Although the IC_{50}s values in HeLa and G-361 cells were very similar, we chose HeLa cells for the additional experiments mentioned above. First, we have checked whether our compounds could influence the cell cycle of these cells. As positive controls, we used two microtubule disruptors, colchicine and paclitaxel, which caused cell cycle arrest in G_2/M phase. We compared the effects of our compounds and we found that (+)-isomers **5l** and **5n** blocked the cell cycle of cervical cancer cells at 15 μM and that (+)-**5n** blocked the cell cycle at 7.5 μM (Fig. 5). In addition, (+)-**5n** strongly inhibited the cell cycle in a dose-dependent manner. The racemates at the 15 μM concentration arrested the cell cycle at G_2/M phase by 60% (**5l**) or

83% (**5n**). A 15 μM solution of (+)-**5n** arrested cells at this phase by 68%, which was greater than that of 20 nM paclitaxel (60%).

Based on these results, we selected only the most interesting concentrations of our compounds for additional experiments to demonstrate the cell cycle arrest and/or the influence on the microtubule organization in HeLa cells by western blotting or immunofluorescence analysis.

Moreover, we compared the effect of racemic **5l** and **5n** and also their enantiopure atropisomers with known microtubule disruptors (colchicine, myoseverin, nocodazole, paclitaxel, tubulysin or vincristine) on microtubules of HeLa cells after 24 h of treatment (Fig. 6).

We detected that both (+)-isomers **5l** and **5n** at 10 nM after 24 h affected microtubule organization (Fig. S4†). We also showed in Fig. 7 that 3.75 μM concentration of (+)-**5n** resulted in very similar clusters of microtubules, such as the depolymerization inhibitor paclitaxel at 20 nM (ref. 29) or paclitaxel analogs.[34]

Based on the results in Fig. 7, racemate **5n** and its atropisomers at 3.75 and 15 μM were analyzed for the expression of proteins associated with G_2/M cell cycle arrest and cytoskeleton in HeLa cells by immunoblotting (Fig. 8A). To compare the effects of all tested compounds, colchicine was used as a microtubule polymerization disruptor, and paclitaxel was used as a depolymerization inhibitor. Significant decreases in α- and β-tubulins expression were detected in cells treated with 15 μM of (+)-**5n** and with colchicine, the positive control. In HeLa cells treated with **5n** at 15 μM and (+)-**5n** at both concentrations, we also detected the phosphorylation of histone H3 at Ser10, which is a specific marker of ongoing mitosis in cells. The marker is associated with the condensation and segregation of chromosomes during mitosis. Phosphorylation starts during prophase, and the highest level can be observed during metaphase; then, phosphorylation decreases.[35] We clearly showed that the phosphorylation of histone H3 at Ser10 was detected after treatment with colchicine, paclitaxel, racemate (15 μM) and the (+)-atropisomer (3.75 and 15 μM), but not with the (−)-isomer of **5n** (Fig. 8A). HeLa cells were treated with 15 μM of **5n**, (−)-**5n**, (+)-**5n** for 24 h, then separated into soluble or polymerized fractions of tubulins.[47] Using western blotting, differences between these two fractions were detected (Fig. 8B). (+)-**5n** decreased the level of soluble and polymerized tubulins (α and β), similarly as colchicine.

Moreover, we determined the level of cyclin B1, which functions in complex with Cdk1 during the regulation of the G2/M phase cell cycle checkpoint; this checkpoint stops the transition to mitosis when DNA is damaged.[36] This DNA defect and aberrant spindle formation can lead to mitotic catastrophe, which is a type of cell death that can occur during mitosis. Mitotic catastrophe can be characterized as a poorly defined type of apoptosis associated with abnormal activation of mitotic kinases and caspases. Mitotic catastrophe is regulated by cell cycle-specific kinases (such as the cyclin B1-dependent kinase Cdk1, polo-like kinases and Aurora kinases), cell cycle checkpoint proteins, members of the Bcl-2 family, survivin, p53, and caspases.[37] The cross-talk and interdependence between Cdk1/cyclin B1-mediated phosphorylation and inactivation of antiapoptotic Bcl-2 proteins was confirmed.[38] Accumulation of cyclin B1, activation of Cdc2/cyclin B1 kinase and Bcl-2 phosphorylation were tightly linked with M phase

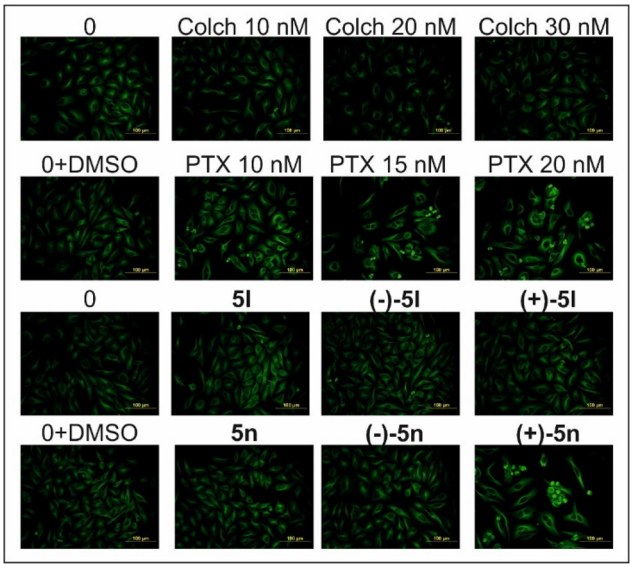

Fig. 7 Effects of racemic and their enantiopure atropisomers on microtubule organization in HeLa cells treated for 24 h with 3.75 μM solutions of **5l** and **5n**. 0 indicates untreated cells, and 0 + DMSO indicates control cells with DMSO at the same level as in the treatment. Colchicine (Colch) and paclitaxel (PTX) were used as positive controls.

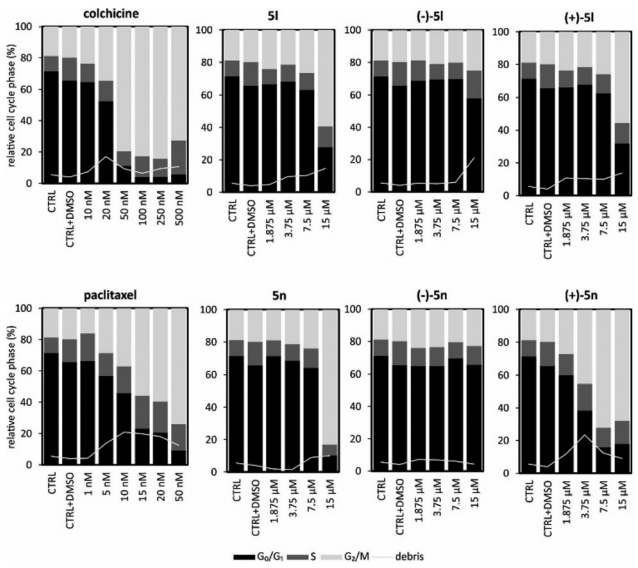

Fig. 6 Changes in the cell cycle detected by flow cytometry. HeLa cells were treated for 24 h with 1.875, 3.75, 7.5, and 15 μM solutions of **5l** and **5n** and their atropisomers. The CTRL bars are control untreated cells, and the CTRL + DMSO bars are control cells treated with DMSO at the same level as in the treatment. Colchicine and paclitaxel were used as positive controls.

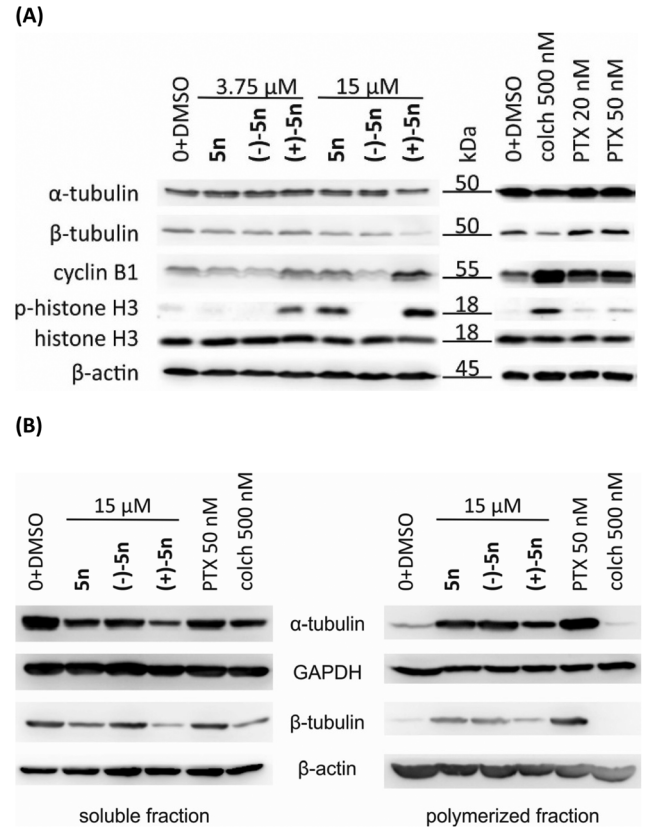

Fig. 8 Comparison of effects of racemate **5n** and its atropisomers with anti-tubulin agents by western blotting. (A) HeLa cells were treated for 24 h with the 3.75 and 15 μM solutions of **5n**. (B) HeLa cells were treated for 24 h with 15 μM solutions of **5n**, then separated into soluble a polymerized fractions. β-Actin or GAPDH was used as loading control. 0 + DMSO are control cells with DMSO in the same level as in the treatment. Colchicine (colch) and paclitaxel (PTX) were used as positive controls.

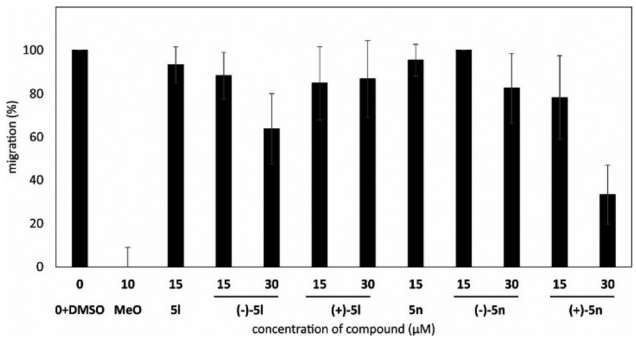

Fig. 9 Inhibition of migration of HUVECs treated for 8 h with 15 and 30 μM solutions of **5l** and **5n**. The ctrl bars are control untreated cells, and the 0 + DMSO bars are control cells treated with DMSO at the same level. 2-Methoxyestradiol (MeO) was used as the positive control. The results presented here are based on a representative experiment that was repeated three times.

arrest but not with apoptosis.[39] These effects, elevated level of cyclin B1 and phosphorylation of Bcl-2, were detected in HeLa cells treated with 3.75 and 15 μM (+)-**5n**, colchicine and paclitaxel (Fig. 4 and 8).

Mitotic catastrophe can be induced by DNA damage, microtubule-depolymerizing agents (such as colchicine, the Vinca alkaloids, cryptophyscins, halichondrins, and estramustine) and by microtubule-hyperpolymerizing agents (taxanes, laulimalide, docodermolide, elutherobins, epothilones, and sarcodictyins).[40] Chromosomes decondense, form random clusters and accumulate in an abnormal metaphase in the presence of paclitaxel.[41]

In HeLa cells, paclitaxel at low concentrations (10 nM for 20 h) suppressed the dynamics of spindle microtubules and therefore arrested cells in mitosis at the metaphase/anaphase transition (by 90%). Paclitaxel did not change the mass of polymerized microtubules but blocked mitosis by kinetically stabilizing spindle microtubules.[42] Colchicine blocked the assembly and polymerization of microtubules by forming tubulin-colchicine complexes. They bind to the ends of microtubules to prevent elongation of the microtubule polymer. Colchicine arrested microtubule growth at low concentrations and promoted microtubule depolymerization at higher concentrations. Colchicine could block mitotic cells in metaphase.[43] Overall, we demonstrated that our compounds exhibit a similar effect to the anti-tubulin agents paclitaxel and colchicine (Fig. 4, 7, and 8). Based on these results, we would like to prove the direct effect of our compounds on tubulin polymerization using fluorescence polymerization assay. Unfortunately, the inhibition of polymerization by (+)-**5n** was not significant in comparison with untreated control and/or positive controls colchicine and paclitaxel (Fig. S5†). We assume that the anti-tubulin effect of (+)-**5n** is probably secondary arising from apoptosis after cell arresting or indirect as described in Zhou *et al.*, 2002.[44]

Atropisomers inhibited migration of endothelial cells. In addition, we determined whether benzimidazoles **5l** and **5n** and their atropisomers influence the migration of human umbilical vein endothelial cells (HUVECs). Atropisomers at 15 and 30 μM of (−)-**5l**, (−)-**5n**, and (+)-**5n** inhibited the dose-dependent migration of HUVECs after 8 h (Fig. 9).

Atropisomers (−)-**5l**, (−)-**5n** and (+)-**5n** inhibited the dose-dependent migration of HUVECs after 8 h. In comparison with the 2-aminobenzimidazole-based compound that significantly inhibited VEGF-A-induced HUVEC migration,[6] our atropisomers showed a weaker effect than the reported inhibitor. Therefore, we assumed that the inhibition of migration *in vitro* is a side effect of their antiproliferative activity.

Conclusions

In summary, we synthesized and investigated the biological activity of new atropisomeric 1-phenylbenzimidazoles, and we revealed differences in cytotoxicity caused by atropisomerism. The association of the *ortho*-substituted phenyl with the presence of strong cytotoxicity in cancer cells and the preservation of inactivity on normal cells was demonstrated. The two best compounds were separated into individual atropisomers, and

their good stability and different biological effects strengthen the activities of (+)-atropisomers. Racemates and single atropisomers arrested the cell cycle, caused apoptosis, and affected the microtubule organization in cancer cells *in vitro* with different intensities. We demonstrated that our compounds exhibit a similar effect to the anti-tubulin agents paclitaxel and colchicine. Therefore, axially chiral benzimidazole **(+)-5n** is promising for the future research.

Experimental

Chemistry

General information. All used chemicals were purchased from VWR, Sigma-Aldrich, Fluorochem, or Acros Organics. All reactions were carried out under regular conditions without any specific precautions to exclude moisture or air from the reaction mixture. The reaction workup and column chromatography were performed with commercial solvents. ^{1}H NMR and ^{13}C NMR spectra were measured on a Jeol ECA400II (400 MHz) in $CDCl_3$ or DMSO-d_6 as a solvent, and referred to the residual nondeuterated solvent peak (7.26 and 77.16 ppm for $CDCl_3$ and 2.50 and 39.52 ppm for DMSO-d_6). The reactions were monitored with analytical thin layer chromatography (TLC), performed on Kieselgel 60 F254 plates (Merck) and visualized by UV light (254 nm). Flash chromatography was performed using silica gel (35–70 μm particle size) column chromatography. HRMS analysis was performed using an LC-MS Orbitrap Elite high-resolution mass spectrometer with electrospray ionization (Dionex Ultimate 3000, Thermo Exactive Plus). The samples were dissolved in MeOH or acetonitrile and injected into the mass spectrometer over the autosampler after HPLC separation; the precolumn was a Phenomenex Gemini (C18, 50 × 2 mm, 2.6 μm) and the isocratic mobile phase MeOH/water/HCOOH 95 : 5 : 0.1. Resolution of selected axially chiral benzimidazoles and racemization stability was carried out on HPLC Agilent 1100 MWD with column Chiralpak IA-3, 3 μm, 4.6mm × 100mm; mobile phase *n*-heptan/ethanol 90 : 10, flow 0.5–1 mL min^{-1}. For semi-preparative isolation of each atropisomer (for compounds **5n** and **5l**) Lux Cellulose-1 column (Phenomenex) 250 × 10 mm, 5 μm particle size was used with mobile phases in isocratic mode: hexane/ethanol 9 : 1 (v/v), 15 min analysis time for **5l** and hexane/methanol/ethanol 40 : 1 : 1 (v/v/v), 35 min analysis time for **5n**.

General synthetic procedures

General method (a). *ortho*-Substituted aniline (5.7 mmol) was dissolved in DMSO (11 mL), then substituted 1-fluoro-2-nitrobenzene (5.7 mmol) and potassium hydroxide (22.8 mmol) were added. The reaction mixture was stirred for 4–12 h at room temperature, then added dropwise to ice water (80 mL) and neutralized with hydrochloric acid at pH 7. The desired nitroaniline was filtered off to give a crude product with sufficient purity for the next step.

General method (b). Compound **3** or **6** (10 mmol) was dissolved in glacial acetic acid (450 mL). 500 mg of 10% palladium on activated charcoal were weighed into a three-necked flask in a hydrogen reduction apparatus and then, a solution of the starting material in acetic acid was added. The reaction mixture was stirred at room temperature in hydrogen atmosphere for 1.5 h. After completion of the reaction, palladium on activated charcoal was removed by filtration. The filtrate was diluted with water (200 mL) and extracted twice with dichloromethane (2 × 100 mL). Then, the dichloromethane solution was three times washed with a 5% aqueous solution of sodium bicarbonate (50 mL) and water (50 mL). Organic phase was evaporated on a rotovap to give a crude product.

General method (c). Compound **3**, **6** or **9** (12.5 mmol) was dissolved in methanol (50 mL) and then zinc (50 mmol) was added. Glacial acetic acid (12.5 mL) was added dropwise to the mixture and the reaction mixture was stirred 15–60 min. The reaction mixture was filtered and the filtrate was poured into water (150 mL). Then, an 5% aqueous solution of sodium bicarbonate was added dropwise to reach pH 7. A solution was extracted three times with CH_2Cl_2, then with brine, and resulting organic phase was dried over $MgSO_4$ and evaporated on a rotovap. The crude product was purified by column chromatography (DCM : hexane).

General method (d). Nitroaniline **3** (3.7 mmol), boronic acid (4.4 mmol), and tripotassium phosphate (7.4 mmol) were dissolved in dioxane (14.5 mL) and water (3.5 mL). After all components were dissolved, XPhos Pd G2 (0.02 mmol, 0.5 mol%) was added and the reaction mixture was heated at 100 °C for 2.5 h. Upon completion, the reaction mixture was acidified with diluted hydrochloric acid (50 mL, 1 : 10). The product was extracted with dichloromethane (3 × 30 mL), the organic phase was dried over $MgSO_4$ and evaporated on a rotovap. A crude product was purified on column chromatography (EtOAc : hexane or DCM : hexane).

General method (e). After reduction (Method b or c), trimethyl orthoformate (10–20 eq.) was added to the reaction mixture, which was stirred at room temperature overnight. After completion of the cyclization, the palladium on activated charcoal or zinc salts were filtered-off. The solvent was evaporated on a rotovap and the residue was dissolved in dichloromethane, washed with an 5% aqueous solution of sodium bicarbonate and water. The organic phase was dried over $MgSO_4$ and a solvent was evaporated on a rotovap. The crude product was purified by column chromatography (EtOAc : hexane or DCM : MeOH).

General method (f). Phenylendiamine **4** or **7** (0.33 mmol) was dissolved in dichloromethane (2 mL). Then, trimethyl orthoformate (3.33 mmol) and *p*-toluenesulfonic acid (0.17 mmol) were added. The reaction mixture was stirred at room temperature overnight. After that, the solution was diluted with dichloromethane (10 mL) and extracted twice with water (10 mL). The organic phase was evaporated and the crude product was purified by column chromatography (DCM : MeOH).

General method (g). Phenylendiamine **4**, **7**, or **10** (0.33 mmol) was dissolved in dichloromethane (2 mL). Then,

trimethyl orthoacetate (3.33 mmol) and *p*-toluenesulfonic acid (0.17 mmol) were added. The reaction mixture was stirred at room temperature overnight. After that, the solution was diluted with dichloromethane (10 mL) and extracted twice with water (10 mL). The organic phase was evaporated and the crude product was purified by column chromatography (DCM : MeOH).

General method (h). Phenylendiamine **4**, **7**, or **10** (0.33 mmol) was dissolved in dichloromethane (2 mL). Then, trimethyl orthobenzoate (3.33 mmol) and *p*-toluenesulfonic acid (0.17 mmol) were added. The reaction mixture was stirred at room temperature overnight. After that, the solution was diluted with dichloromethane (10 mL) and washed twice with water (10 mL). The organic phase was evaporated and the crude product was purified by column chromatography (DCM : MeOH).

1-(2-Iodophenyl)-7-methyl-1*H*-benzo[*d*]imidazole (5a). Prepared by method (**e**). A light brown solid (100 mg, 86%, m.p. 140–142 °C). ^{1}H NMR (400 MHz, $CDCl_3$) δ = 8.02 (dd, J = 7.9, 1.2 Hz, 1H), 7.84 (s, 1H), 7.75 (dd, J = 7.9, 1.2 Hz, 1H), 7.47–7.55 (m, 2H), 7.27–7.30 (m, 1H), 7.22–7.27 (m, 1H), 7.04 (dd, J = 7.3, 0.9 Hz, 1H), 1.99 (s, 3H) ppm. ^{13}C NMR (101 MHz, $CDCl_3$) δ = 143.5, 143.1, 140.4, 139.4, 132.8, 131.1, 129.7, 129.0, 125.6, 122.8, 121.8, 118.4, 99.5, 17.6 ppm. HRMS (ESI): m/z calcd $C_{14}H_{11}IN_2$ for $[M + H]^+$ 335.0040, found 335.0037.

7-Chloro-1-(2-(trifluoromethyl)phenyl)-1*H*-benzo[*d*]imidazole (5b). Prepared by method (**e**). A white solid (74 mg, 50%, m.p. 73–75 °C). ^{1}H NMR (400 MHz, DMSO-d_6) δ = 8.46 (s, 1H), 8.00 (dd, J = 7.6, 1.8 Hz, 1H), 7.82–7.92 (m, 2H), 7.80 (dd, J = 7.8, 1.4 Hz, 1H), 7.77 (dd, J = 6.7, 2.4 Hz, 1H), 7.26–7.32 (m, 2H) ppm. ^{13}C NMR (101 MHz, $CDCl_3$) δ = 144.8, 144.7, 134.2 (q, J = 1.5 Hz) 132.4, 131.9, 131.6, 130.2, 129.1 (q, J = 30.8 Hz) 126.8 (q, J = 4.6 Hz) 124.9, 123.5, 122.8 (q, J = 273.8 Hz) 119.4, 116.7 ppm. HRMS (ESI): m/z calcd $C_{14}H_8ClF_3N_2$ for $[M + H]^+$ 297.0401, found 297.0398.

7-Chloro-1-(2-iodophenyl)-1*H*-benzo[*d*]imidazole (5c). Prepared by method (**e**). A white solid (35 mg, 86%, m.p. 156–159 °C). ^{1}H NMR (400 MHz, $CDCl_3$) δ = 8.00 (dd, J = 8.1, 1.4 Hz, 1H), 7.89 (s, 1H), 7.79–7.84 (m, 1H), 7.46–7.54 (m, 2H), 7.25–7.29 (m, 3H) ppm. ^{13}C NMR (101 MHz, $CDCl_3$) δ = 145.1, 144.0, 139.3, 139.2, 131.2, 129.7, 128.8, 124.8, 123.4, 119.4, 116.9, 99.9, 99.4 ppm. HRMS (ESI): m/z calcd $C_{13}H_8ClIN_2$ for $[M + H]^+$ 354.9493 found 354.9492.

1-(2-Iodophenyl)-7-(trifluoromethyl)-1*H*-benzo[d]imidazole (5d). Prepared by method (**e**). A white solid (177 mg, 87%, m.p. 95–98 °C). ^{1}H NMR (400 MHz, $CDCl_3$) δ = 8.11 (d, J = 8.2 Hz, 1H), 8.01 (dd, J = 7.9, 1.2 Hz, 1H), 7.91 (s, 1H), 7.65 (d, J = 7.6 Hz, 1H), 7.47–7.56 (m, 2H), 7.40–7.46 (m, 1H), 7.28 (ddd, J = 7.9, 7.0, 2.1 Hz, 1H) ppm. ^{13}C NMR (101 MHz, $CDCl_3$) δ = 145.5, 145.4, 139.5, 139.2, 131.4, 130.2, 129.8 (q, J = 1.0 Hz) 128.9, 124.9, 123.0 (q, J = 272.3 Hz), 122.2 (q, J = 5.5 Hz), 114.6 (q, J = 35.2 Hz) 99.2, 91.4 ppm. HRMS (ESI): m/z calcd $C_{14}H_8F_3IN_2$ for $[M + H]^+$ 388.9757, found 388.9756.

Methyl 2-(7-chloro-1*H*-benzo[*d*]imidazol-1-yl)benzoate (5e). Prepared by method (**e**). A light brown solid (47 mg, 49%, m.p. 300–304 °C). ^{1}H NMR (400 MHz, $CDCl_3$) δ = 8.95 (s, 1H), 7.99 (dd, J = 7.9, 1.2 Hz, 1H), 7.27–7.31 (m, 1H), 7.02–7.07 (m, 1H), 6.87 (dd, J = 8.1, 1.4 Hz, 1H), 6.70–6.77 (m, 2H), 6.39 (dd, J = 8.4, 0.8 Hz, 1H), 3.95 (s, 3H) ppm. ^{13}C NMR (101 MHz, $CDCl_3$) δ = 169.0, 148.7, 146.0, 134.5, 134.0, 131.4, 128.0, 123.0, 119.1, 117.1, 113.7, 113.4, 111.5, 93.1, 51.8 ppm. HRMS (ESI): m/z calcd $C_{15}H_{11}ClN_2O_2$ for $[M + H]^+$ 287.0582, found 287.0574.

1-(2-Bromophenyl)-7-chloro-1*H*-benzo[*d*]imidazole (5f). Prepared by method (**e**). A light brown solid (74 mg, 72%, m.p. 110–113 °C). ^{1}H NMR (400 MHz, $CDCl_3$) δ = 7.90 (s, 1H), 7.78–7.82 (m, 1H), 7.74–7.77 (m, 1H), 7.47–7.50 (m, 2H), 7.42–7.45 (m, 1H), 7.26 (m, 2H) ppm. ^{13}C NMR (101 MHz, $CDCl_3$) δ = 144.2, 135.7, 133.1, 132.7, 131.1, 130.4, 127.9, 124.8, 123.8, 123.4, 119.4, 116.8, 95.2 ppm. HRMS (ESI): m/z calcd $C_{13}H_8BrClN_2$ for $[M + H]^+$ 306.9632, found 306.9633.

2-(7-Chloro-1*H*-benzo[*d*]imidazol-1-yl)benzonitrile (5g). Prepared by method (**f**). A white solid (57 mg, 68%, m.p. 104–106 °C). ^{1}H NMR (400 MHz, $CDCl_3$) δ = 7.95 (s, 1H), 7.81–7.84 (m, 1H), 7.79 (t, J = 4.58 Hz, 1H), 7.73 (dd, J = 7.78, 1.68 Hz, 1H), 7.64 (dd, J = 7.63, 1.22 Hz, 1H), 7.53 (dd, J = 7.93, 1.22 Hz, 1H), 7.25–7.27 (m, 2H) ppm. ^{13}C NMR (101 MHz, $CDCl_3$) δ = 145.3, 143.8, 138.5, 133.3, 130.7, 129.9, 129.8, 125.4, 124.0, 119.8, 116.5, 115.1, 113.1, 101.2 ppm. HRMS (ESI): m/z calcd $C_{14}H_8ClN_3$ for $[M + H]^+$ 254.0480, found 254.0479.

2-(2-Methyl-1*H*-benzo[*d*]imidazol-1-yl)benzoic acid (5h). Prepared by method (**g**). A white solid (94 mg, 75%, m.p. 240–242 °C). ^{1}H NMR (400 MHz, DMSO-d_6) δ = 8.08 (dd, J = 7.9, 1.5 Hz, 1H), 7.83 (td, J = 7.6, 1.2 Hz, 1H), 7.72 (td, J = 7.6, 1.2 Hz, 1H), 7.58 (ddd, J = 8.1, 2.6, 0.9 Hz, 2H), 7.09–7.20 (m, 2H), 6.85 (dd, J = 7.8, 1.4 Hz, 1H), 2.29 (s, 3H) ppm. ^{13}C NMR (101 MHz, DMSO-d_6) δ = 166.2, 151.8, 142.3, 136.8, 134.5, 133.5, 131.4, 130.3, 129.9, 129.7, 122.1, 121.5, 118.2, 109.3, 13.8 ppm. HRMS (ESI): m/z calcd $C_{15}H_{12}N_2O_2$ for $[M + H]^+$ 253.0972, found 253.0971.

7-Chloro-1-(2-iodophenyl)-2-methyl-1*H*-benzo[*d*]imidazole (5i). Prepared by method (**g**). A light brown solid (80 mg, 81%, m.p. 152–153 °C). ^{1}H NMR (400 MHz, $CDCl_3$) δ = 8.01 (dd, J = 7.9, 1.2 Hz, 1H), 7.68 (dd, J = 7.6, 1.2 Hz, 1H), 7.53 (td, J = 7.6, 1.2 Hz, 1H), 7.43 (dd, J = 7.9, 1.4 Hz, 1H), 7.25–7.30 (m, 1H), 7.15–7.23 (m, 2H), 2.37 (s, 3H) ppm. ^{13}C NMR (101 MHz, $CDCl_3$) δ = 152.6, 144.4, 139.4, 131.4, 131.1, 130.0, 129.1, 124.0, 123.0, 118.5, 118.0, 116.1, 100.1, 14.3 ppm. HRMS (ESI): m/z calcd $C_{14}H_{10}ClIN_2$ for $[M + H]^+$ 368.9650, found 368.9648.

1-(2-Iodophenyl)-2-methyl-1*H*-benzo[*d*]imidazole (5j). Prepared by method (**g**). A light brown solid (85 mg, 77%, m.p. 127–130 °C). ^{1}H NMR (400 MHz, $CDCl_3$) δ = 8.08 (dd, J = 8.1, 1.4 Hz, 1H), 7.78 (d, J = 7.9 Hz, 1H), 7.57 (td, J = 7.6, 1.2 Hz, 1H), 7.38 (dd, J = 7.6, 1.5 Hz, 1H), 7.26–7.32 (m, 2H), 7.21 (ddd, J = 8.1, 7.1, 1.2 Hz, 1H), 6.89–6.92 (m, 1H), 2.44 (s, 3H) ppm. ^{13}C NMR (101 MHz, $CDCl_3$) δ = 151.3, 140.4, 138.9, 135.9, 131.2, 131.1, 129.8, 129.4, 122.7, 122.5, 119.1, 110.0, 98.6, 14.4 ppm. HRMS (ESI): m/z calcd $C_{14}H_{11}IN_2$ for $[M + H]^+$ 335.0040, found 335.0025.

2-(7-Chloro-2-methyl-1*H*-benzo[*d*]imidazol-1-yl)benzonitrile (5k). Prepared by method (**g**). A white solid (71 mg, 80%,

m.p. 103–106 °C). ^{1}H NMR (400 MHz, $CDCl_3$) δ = 7.88 (dd, J = 7.6, 1.5 Hz, 1H), 7.79 (td, J = 7.6, 1.5 Hz, 1H), 7.66–7.71 (m, 2H), 7.50 (dd, J = 7.9, 1.2 Hz, 1H), 7.17–7.25 (m, 2H), 2.42 (s, 3H) ppm. ^{13}C NMR (101 MHz, $CDCl_3$) δ = 152.5, 144.6, 139.1, 133.5, 133.4, 132.0, 130.5, 130.2, 124.3, 123.5, 118.4, 115.7, 115.0, 114.0, 14.1 ppm. HRMS (ESI): m/z calcd $C_{15}H_{10}ClN_3$ for $[M + H]^+$ 268.0636, found 268.0635.

7-Chloro-1-(2-iodophenyl)-2-phenyl-1*H*-benzo[*d*]imidazole (5l). Prepared by method (**h**). A white solid (148 mg, 57%, m.p. 143–145 °C). ^{1}H NMR (400 MHz, $CDCl_3$) δ = 7.94 (dd, J = 7.9, 1.2 Hz, 1H), 7.83 (dd, J = 7.5, 1.4 Hz, 1H), 7.55–7.62 (m, 2H), 7.42–7.49 (m, 2H), 7.20–7.37 (m, 6H) ppm. ^{13}C NMR (101 MHz, $CDCl_3$) δ = 153.2, 144.7, 140.0, 139.3, 131.9, 131.1, 131.0, 129.8, 129.52, 129.48, 128.8, 128.3, 124.9, 123.5, 118.9, 116.7, 101.3 ppm. HRMS (ESI): m/z calcd $C_{19}H_{12}ClIN_2$ for $[M + H]^+$ 430.9806, found 430.9803. For separation method and X-Ray structure determination see ESI.† (S_a)-(−)-7-Chloro-1-(2-iodophenyl)-2-phenyl-1*H*-benzo[*d*]imidazole **(−)-5l**: $[\alpha]_D^{22}$ −49.5° (c = 0.20 g per 100 mL, DCM), (R_a)-(+)-7-Chloro-1-(2-iodophenyl)-2-phenyl-1*H*-benzo[*d*]imidazole **(+)-5l**: $[\alpha]_D^{22}$ +49.5° (c = 0.20 g per 100mL, DCM).

1-(2-Iodophenyl)-2-phenyl-7-(trifluoromethyl)-1*H*-benzo[*d*]imidazole (5m). Prepared by method (**h**). A white solid (72 mg, 62%, m.p. 192–195 °C). ^{1}H NMR (400 MHz, $CDCl_3$) δ = 8.12 (d, J = 7.9 Hz, 1H), 7.85 (dd, J = 8.1, 1.4 Hz, 1H), 7.67–7.71 (m, 1H), 7.64 (d, J = 7.6 Hz, 1H), 7.54–7.58 (m, 2H), 7.52 (td, J = 7.6, 1.2 Hz, 1H), 7.41–7.46 (m, 1H), 7.33–7.38 (m, 1H), 7.27–7.32 (m, 2H), 7.19 (td, J = 7.8, 1.5 Hz, 1H) ppm. ^{13}C NMR (101 MHz, $CDCl_3$) δ = 154.7, 144.9, 139.7, 132.1, 131.5, 131.1, 129.8, 129.7, 128.5, 128.1, 127.0, 124.5, 123.0 (q, J = 272.3 Hz), 122.2, 122.0, 118.9, 114.6 (q, J = 34.6 Hz) 100.6 (q, J = 1.4 Hz) ppm. HRMS (ESI): m/z calcd $C_{20}H_{12}F_3IN_2$ for $[M + H]^+$ 465.0070, found 465.0075.

2-(7-Chloro-2-phenyl-1*H*-benzo[*d*]imidazol-1-yl)benzonitrile (5n). Prepared by method (**h**). A white solid (82 mg, 75%, m.p. 180–182 °C). ^{1}H NMR (400 MHz, $CDCl_3$) δ = 7.84 (dd, J = 7.6, 1.5 Hz, 1H), 7.77 (dd, J = 7.6, 1.5 Hz, 1H), 7.70 (td, J = 7.9, 1.5 Hz, 1H), 7.61 (td, J = 7.6, 1.5 Hz, 1H), 7.49–7.55 (m, 3H), 7.36–7.41 (m, 1H), 7.26–7.34 (m, 4H) ppm. ^{13}C NMR (101 MHz, $CDCl_3$) δ = 153.9, 145.0, 139.8, 133.1, 133.1, 132.5, 131.4, 130.0, 129.9, 129.5, 129.0, 128.5, 125.2, 123.9, 119.3, 116.2, 115.1, 114.7 ppm. HRMS (ESI): m/z calcd $C_{20}H_{12}ClN_3$ for $[M + H]^+$ 330.0793, found 330.0787. For separation method and X-ray structure determination see ESI.† (S_a)-(−)-2-(7-Chloro-2-phenyl-1*H*-benzo[*d*]imidazol-1-yl)benzonitrile **(−)-5n**: $[\alpha]_D^{22}$ −12.5° (c = 0.15 g per 100 mL, DCM), (R_a)-(+)-2-(7-Chloro-2-phenyl-1*H*-benzo[*d*]imidazol-1-yl)benzonitrile **(+)-5n**: $[\alpha]_D^{22}$ + 12.5° (c = 0.15 g per 100 mL, DCM).

7-Chloro-1,2-diphenyl-1*H*-benzo[*d*]imidazole (5o). Prepared by method (**h**). A light brown solid (35 mg, 40%, m.p. 142–146 °C). ^{1}H NMR (400 MHz, $CDCl_3$) δ = 7.81 (dd, J = 7.3, 2.4 Hz, 1H), 7.42–7.54 (m, 5H), 7.31–7.41 (m, 3H), 7.23–7.30 (m, 4H) ppm. ^{13}C NMR (101 MHz, $CDCl_3$) δ = 154.0, 144.8, 137.0, 132.8, 129.8, 129.7, 129.6, 129.3, 128.8, 128.2, 124.9, 123.2, 118.7, 116.7, 91.9 ppm. HRMS (ESI): m/z calcd $C_{19}H_{13}ClN_2$ for $[M + H]^+$ 305.0840, found 305.0837.

2-(7-(*p*-Tolyl)-1*H*-benzo[*d*]imidazol-1-yl)benzonitrile (8a). Prepared by method (**e**). A white solid (263 mg, 85%, m.p. 175 °C). ^{1}H NMR (400 MHz, DMSO-d_6) δ = 8.50 (s, 1H), 7.82 (dd, J = 8.0, 1.1 Hz, 1H), 7.63 (dd, J = 7.6, 1.1 Hz, 1H), 7.53–7.58 (m, 1H), 7.38–7.48 (m, 3H), 7.19 (dd, J = 7.3, 0.9 Hz, 1H), 6.80–6.88 (m, 4H), 2.17 (s, 3H) ppm. ^{13}C NMR (101 MHz, DMSO-d_6) δ = 145.0, 143.9, 138.9, 136.0, 133.7, 133.6, 132.8, 131.3, 128.8, 128.7, 128.7, 127.9, 127.1, 125.1, 122.8, 119.1, 115.7, 110.5, 20.6 ppm. HRMS (ESI): m/z calcd $C_{21}H_{15}N_3$ for $[M + H]^+$ 310.1339, found 310.1340.

2-(7-(4-Hydroxyphenyl)-1*H*-benzo[*d*]imidazol-1-yl)benzonitrile (8b). Prepared by method (**e**). A colourless oil (46 mg, 52%). ^{1}H NMR (400 MHz, DMSO-d_6) δ = 9.31 (s, 1H), 8.47 (s, 1H), 7.78 (dd, J = 8.0, 1.1 Hz, 1H), 7.68 (dd, J = 7.8, 1.4 Hz, 1H), 7.57–7.62 (m, 1H), 7.47 (td, J = 7.7, 1.1 Hz, 1H), 7.43 (dd, J = 7.8, 0.9 Hz, 1H), 7.37 (td, J = 7.8, 0.9 Hz, 1H), 7.15 (dd, J = 7.3, 0.9 Hz, 1H), 6.78 (d, J = 8.7 Hz, 2H), 6.40 (d, J = 8.7 Hz, 2H) ppm. ^{13}C NMR (101 MHz, DMSO-d_6) δ = 156.2, 144.9, 143.9, 138.9, 133.6, 132.8, 131.3, 129.8, 128.9, 128.7, 127.2, 127.1, 125.2, 122.7, 118.6, 115.6, 114.1, 110.5 ppm. HRMS (ESI): m/z calcd $C_{20}H_{13}N_3O$ for $[M + H]^+$ 312.1131, found 312.1131.

2-(7-(4-Methoxyphenyl)-1*H*-benzo[*d*]imidazol-1-yl)benzonitrile (8c). Prepared by method (**f**). A white solid (15 mg, 16%, m.p. 217–220 °C). ^{1}H NMR (400 MHz, $CDCl_3$) δ = 8.05 (s, 1H), 7.91 (dd, J = 7.9, 1.0 Hz, 1H), 7.50–7.53 (m, 1H), 7.43 (td, J = 7.6, 0.9 Hz, 1H), 7.31–7.35 (m, 2H), 7.26 (dd, J = 7.4, 1.2 Hz, 1H), 7.02–7.05 (m, 1H), 6.95–6.98 (m, 2H), 6.55–6.58 (m, 2H), 3.73 (s, 3H) ppm. ^{13}C NMR (101 MHz, $CDCl_3$) δ = 158.7, 144.0, 143.9, 138.9, 133.01, 132.95, 130.2, 129.2, 128.6, 128.4, 127.1, 126.4, 123.9, 119.4, 115.2, 113.1, 111.0, 55.3 ppm. HRMS (ESI): m/z calcd $C_{21}H_{15}N_3O$ for $[M + H]^+$ 326.1288, found 326.1284.

2-(7-(Thiophen-3-yl)-1*H*-benzo[*d*]imidazol-1-yl)benzonitrile (8d). Prepared by method (**f**). A white solid (22 mg, 24%, m.p. 155–157 °C). ^{1}H NMR (500 MHz, $CDCl_3$) δ = 8.07 (s, 1H), 7.93 (dd, J = 8.0, 0.9 Hz, 1H), 7.57–7.59 (m, 1H), 7.37–7.45 (m, 3H), 7.31 (dd, J = 7.3, 0.7 Hz, 1H), 7.08–7.11 (m, 1H), 6.90–6.95 (m, 2H), 6.67 (dd, J = 4.9, 1.2 Hz, 1H) ppm. ^{13}C NMR (126 MHz, $CDCl_3$) δ = 143.6, 139.0, 137.7, 133.2, 133.0, 129.9, 129.8, 128.5, 128.5, 127.9, 126.1, 125.4, 124.6, 123.3, 121.9, 120.3, 115.4, 110.7 ppm. HRMS (ESI): m/z calcd $C_{18}H_{11}N_3S$ for $[M + H]^+$ 302.0746, found 302.0746.

2-(7-Phenyl-1*H*-benzo[*d*]imidazol-1-yl)benzonitrile (8e). Prepared by method (**f**). A white solid (83 mg, 80%, m.p. 214–216 °C). ^{1}H NMR (400 MHz, $CDCl_3$) δ = 8.04 (s, 1H), 7.93 (dd, J = 8.1, 1.1 Hz, 1H), 7.42–7.50 (m, 2H), 7.26–7.31 (m, 3H), 6.98–7.06 (m, 6H) ppm. ^{13}C NMR (126 MHz, $CDCl_3$) δ = 144.4, 143.6, 139.1, 137.2, 133.0, 132.9, 131.4, 129.0, 128.4, 128.2, 127.6, 127.1, 126.9, 126.0, 123.4, 120.0, 115.4, 110.8 ppm. HRMS (ESI): m/z calcd $C_{20}H_{13}N_3$ for $[M + H]^+$ 296.1182, found 296.1181.

2-(2-Methyl-7-(*p*-tolyl)-1*H*-benzo[*d*]imidazol-1-yl)benzonitrile (8f). Prepared by method (**g**). A white solid (259 mg, 80%, m.p. 198–200 °C). ^{1}H NMR (400 MHz, DMSO-d_6) δ = 7.68 (dd, J = 8.2, 0.9 Hz, 1H), 7.58–7.63 (m, 2H), 7.51–7.54 (m, 1H), 7.43–7.48 (m, 1H), 7.29–7.34 (m, 1H), 7.05 (dd, J = 7.6, 1.2 Hz, 1H), 6.76–6.83 (m, 4H), 2.31 (s, 3H), 2.16 (s, 3H) ppm. ^{13}C

NMR (101 MHz, DMSO-d_6) δ = 151.9, 143.0, 139.0, 135.8, 134.0, 133.4, 133.1, 132.8, 130.0, 129.2, 128.7, 127.8, 126.5, 124.5, 122.2, 117.9, 115.6, 111.5, 20.6, 14.0 ppm. HRMS (ESI): *m*/*z* calcd $C_{22}H_{17}N_3$ for $[M + H]^+$ 324.1495, found 324.1492.

2-(7-(4-Methoxyphenyl)-2-methyl-1*H*-benzo[*d*]imidazol-1-yl) benzonitrile (8g). Prepared by method (**g**). A white solid (61 mg, 71%, m.p. 210–213 °C). ^{1}H NMR (500 MHz, $CDCl_3$) δ = 7.79 (dd, *J* = 8.2, 1.0 Hz, 1H), 7.51 (dd, *J* = 7.5, 1.7 Hz, 1H), 7.31–7.39 (m, 3H), 7.12 (dd, *J* = 7.3, 1.0 Hz, 1H), 7.01 (dd, *J* = 8.0, 1.2 Hz, 1H), 6.91 (d, *J* = 8.6 Hz, 2H), 6.53 (d, *J* = 8.9 Hz, 2H), 3.72 (s, 3H), 2.45 (s, 3H) ppm. ^{13}C NMR (126 MHz, $CDCl_3$) δ = 158.3, 152.0, 143.4, 139.8, 133.4, 133.1, 133.1, 130.2, 129.7, 129.5, 128.7, 126.3, 125.3, 122.7, 118.5, 115.4, 112.9, 112.8, 55.3, 14.3 ppm. HRMS (ESI): *m*/*z* calcd $C_{22}H_{17}N_3O$ for $[M + H]^+$ 340.1444, found 340.1446.

2-(2-Methyl-7-(thiophen-3-yl)-1*H*-benzo[*d*]imidazol-1-yl)benzonitrile (8h). Prepared by method (**g**). A white solid (65 mg, 67%, m.p. 196–199 °C). ^{1}H NMR (500 MHz, $CDCl_3$) δ = 7.80 (dd, *J* = 8.2, 1.0 Hz, 1H), 7.57 (dd, *J* = 7.7, 1.7 Hz, 1H), 7.37–7.46 (m, 2H), 7.34 (t, *J* = 7.7 Hz, 1H), 7.16 (dd, *J* = 7.3, 1.0 Hz, 1H), 7.07 (dd, *J* = 7.9, 1.0 Hz, 1H), 6.86–6.90 (m, 2H), 6.61 (dd, *J* = 4.7, 1.3 Hz, 1H), 2.45 (s, 3H) ppm. ^{13}C NMR (126 MHz, $CDCl_3$) δ = 152.1, 143.4, 139.5, 137.5, 133.4, 133.2, 130.1, 129.3, 128.9, 128.6, 125.4, 124.3, 123.2, 122.6, 121.2, 119.0, 115.4, 112.6, 14.3 ppm. HRMS (ESI): *m*/*z* calcd $C_{19}H_{13}N_3S$ for $[M + H]^+$ 316.0903, found 316.0901.

2-(2-Methyl-7-phenyl-1*H*-benzo[*d*]imidazol-1-yl)benzonitrile (8i). Prepared by method (**g**). A white solid (79 mg, 73%, m.p. 189–192 °C). ^{1}H NMR (400 MHz, $CDCl_3$) δ = 7.86 (dd, *J* = 8.1, 1.1 Hz, 1H), 7.49 (dd, *J* = 7.6, 1.5 Hz, 1H), 7.34–7.46 (m, 3H), 7.22 (dd, *J* = 7.3, 1.2 Hz, 1H), 7.18 (dd, *J* = 7.8, 1.1 Hz, 1H), 6.98–7.06 (m, 5H), 2.58 (s, 3H) ppm. ^{13}C NMR (101 MHz, $CDCl_3$) δ = 152.0, 139.5, 138.3, 136.2, 133.4, 133.2, 132.0, 129.6, 129.5, 129.1, 127.5, 127.2, 127.0, 126.3, 123.9, 117.5, 115.0, 112.6, 13.7 ppm. HRMS (ESI): *m*/*z* calcd $C_{21}H_{15}N_3$ for $[M + H]^+$ 310.1339, found 310.1339 ppm.

2-(7-(4-Methoxyphenyl)-2-phenyl-1*H*-benzo[*d*]imidazol-1-yl) benzonitrile (8j). Prepared by method (**h**). A white solid (66 mg, 58%, m.p. 233–235 °C). ^{1}H NMR (500 MHz, $CDCl_3$) δ = 7.94 (dd, *J* = 8.3, 1.2 Hz, 1H), 7.39–7.43 (m, 3H), 7.33–7.37 (m, 2H), 7.27–7.29 (m, 3H), 7.25–7.27 (m, 1H), 7.18 (dd, *J* = 7.3, 1.0 Hz, 1H), 7.01–7.04 (m, 1H), 6.89 (d, *J* = 6.9 Hz, 2H), 6.51–6.54 (m, 2H), 3.74 (s, 3H) ppm. ^{13}C NMR (126 MHz, $CDCl_3$) δ = 158.3, 153.2, 143.7, 140.5, 133.7, 132.84, 132.78, 130.39, 130.30, 130.2, 129.7, 129.61, 129.58, 128.5, 128.3, 126.9, 126.3, 123.1, 119.4, 115.3, 113.3, 112.9, 55.3 ppm. HRMS (ESI): *m*/*z* calcd $C_{27}H_{19}N_3O$ for $[M + H]^+$ 402.1601, found 402.1600.

2-(2-Phenyl-7-(thiophen-3-yl)-1*H*-benzo[*d*]imidazol-1-yl)benzonitrile (8k). Prepared by method (**h**). A white solid (75 mg, 64%, m.p. 206–209 °C). ^{1}H NMR (500 MHz, $CDCl_3$) δ = 7.95 (dd, *J* = 8.0, 1.2 Hz, 1H), 7.39–7.44 (m, 4H), 7.32–7.37 (m, 3H), 7.27–7.30 (m, 2H), 7.22 (dd, *J* = 7.5, 1.2 Hz, 1H), 7.08 (dd, *J* = 7.9, 1.3 Hz, 1H), 6.86–6.90 (m, 2H), 6.55–6.57 (m, 1H) ppm. ^{13}C NMR (126 MHz, $CDCl_3$) δ = 153.3, 143.7, 140.2, 137.5, 133.7, 133.0, 132.9, 129.8, 129.7, 129.6, 129.5, 128.7, 128.3, 126.4, 125.2, 124.1, 123.4, 123.0, 121.8, 119.9, 115.3, 113.0 ppm. HRMS (ESI): *m*/*z* calcd $C_{24}H_{15}N_3S$ for $[M + H]^+$ 378.1059, found 378.1059.

2-(2,7-Diphenyl-1*H*-benzo[*d*]imidazol-1-yl)benzonitrile (8l).. Prepared by method (**h**). A white solid (75 mg, 57%, m.p. 188–190 °C). ^{1}H NMR (400 MHz, $CDCl_3$) δ = 7.96 (dd, *J* = 8.1, 1.1 Hz, 1H), 7.40–7.45 (m, 3H), 7.27–7.37 (m, 3H), 7.22–7.27 (m, 3H), 7.20 (dd, *J* = 7.5, 1.1 Hz, 1H), 6.96–7.08 (m, 6H) ppm. ^{13}C NMR (126 MHz, $CDCl_3$) δ = 153.3, 143.8, 140.3, 137.2, 133.4, 132.9, 132.8, 130.1, 129.7, 129.6, 129.5, 129.3, 128.6, 128.3, 127.4, 127.2, 126.6, 126.1, 123.1, 119.6, 115.3, 113.2 ppm. HRMS (ESI): *m*/*z* calcd $C_{26}H_{17}N_3$ for $[M + H]^+$ 372.1495, found 372.1494.

2-Methyl-1-(4′-methyl-[1,1′-biphenyl]-2-yl)-1*H*-benzo[*d*]imidazole (11a). Prepared by method (**g**). A light brown solid (22 mg, 44%, m.p. 142–145 °C). ^{1}H NMR (400 MHz, $CDCl_3$) δ = 7.70 (dd, *J* = 7.3, 0.9 Hz, 1H), 7.57–7.65 (m, 2H), 7.52 (td, *J* = 7.6, 1.9 Hz, 1H), 7.39 (dd, *J* = 7.9, 1.2 Hz, 1H), 7.26 (td, *J* = 7.6, 1.4 Hz, 1H), 7.21 (td, *J* = 7.6, 1.4 Hz, 1H), 7.11–7.15 (m, 1H), 6.96 (dd, *J* = 7.6, 1.0 Hz, 2H), 6.86 (d, *J* = 7.6 Hz, 2H), 2.24 (s, 3H), 2.07 (s, 3H) ppm. ^{13}C NMR (101 MHz, $CDCl_3$) δ = 151.8, 142.7, 140.5, 137.6, 137.2, 134.8, 133.3, 131.5, 129.6, 129.4, 128.8, 128.4, 127.8, 122.4, 122.1, 118.9, 110.0, 21.0, 14.0 ppm. HRMS (ESI): *m*/*z* calcd $C_{21}H_{18}N_2$ for $[M + H]^+$ 299.1543, found 299.1540.

1-(4′-Methyl-[1,1′-biphenyl]-2-yl)-2-phenyl-1*H*-benzo[*d*]imidazole (11b). Prepared by method (**h**). A light brown solid (37 mg, 64%, m.p. 131–134 °C). ^{1}H NMR (400 MHz, $CDCl_3$) δ = 7.84–7.87 (m, 1H), 7.62–7.65 (m, 1H), 7.53–7.60 (m, 2H), 7.41–7.45 (m, 1H), 7.32–7.37 (m, 1H), 7.28–7.32 (m, 2H), 7.22–7.27 (m, 1H), 7.11–7.14 (m, 4H), 6.75 (dd, *J* = 7.9, 0.6 Hz, 2H), 6.32 (d, *J* = 8.2 Hz, 2H), 2.21 (s, 3H) ppm. ^{13}C NMR (101 MHz, $CDCl_3$) δ = 152.4, 142.6, 139.9, 137.2, 136.6, 134.3, 134.0, 131.3, 129.7, 129.0, 128.6, 128.5, 128.14, 128.10, 128.08, 127.4, 127.1, 122.9, 122.4, 119.4, 110.2, 20.6 ppm. HRMS (ESI): *m*/*z* calcd $C_{26}H_{20}N_2$ for $[M + H]^+$ 361.1699, found 361.1700.

Biology

Cell cultures. Cell lines were cultivated under standard cell culture conditions in a 37 °C incubator with a humidified 5% CO_2 atmosphere. Cell culture media (DMEM, Sigma, MO, USA; RPMI, Biowest, France) were supplemented with fetal bovine serum (FBS, Biowest, France), 2 mM L-glutamine (Sigma, MO, USA), 100 μg mL^{-1} streptomycin, and 100 U mL^{-1} penicillin (Sigma, MO, USA). Human foreskin fibroblasts (BJ) were kindly gifted by Jiří Bartek's laboratory (Danish Cancer Society Center, Copenhagen, Denmark) and HUVECs were a kind gift from Jitka Ulrichová (Faculty of Medicine and Dentistry, Palacký University Olomouc). HUVECs were cultured in Endothelial Cell Proliferation Medium (ECPM, Provitro, Berlin, Germany). Other cell lines used in our study were purchased from the European Collection of Authenticated Cell Cultures (ECACC), from the American Type Culture Collection (ATCC) or from Leibniz Institute DSMZ-German Collection of Microorganisms and Cell Cultures (DSMZ). The concentration of FBS and the type of cell culture media varied depending on the cell line (see Table S2 in the ESI†). Cells were washed in phosphate-buffered saline (PBS), adherent cells were released

by the treatment with EGTA/trypsin solution, and subcultured into the fresh medium two to three times per week.

Cytotoxicity assay. Cells were seeded into a 96-well plate one day prior to treatment and then treated in triplicate with a compound diluted in dimethyl sulfoxide (Sigma, MO, USA) to six concentrations by 3-fold dilution. The concentration of DMSO never exceed 0.6%. The cell viability was determined after 72 h of the treatment by the resazurin assay (Sigma, MO, USA) *via* the fluorescence readout at excitation/emission wavelengths 544/590 nm measured by the Fluoroskan Ascent microplate reader (Labsystems, Finland) as described earlier for Calcein AM dye.[45]

Cell cycle analysis. HeLa cells were seeded into 24-well plate (3.5×10^4 cells per well), treated for 24 h and stained as described previously.[38] MV4-11 cells were seeded into a 96-well plate (5×10^4 per well) and treated with a compounds for 24 h.[46] After the incubation period, the 5× concentrated staining solution was added directly to the well with the cells. BD FACSVerse™ flow cytometer with the BD FACS Universal Loader for microplates and BD FACSuite™ software (version 1.0.6) were used to analyze the samples. The dye was excited with the 488 nm laser operating at 20 mW power and the emitted light was detected *via* the 586/42 bandpass filter. The data were processed and the cell cycle distribution was fitted in ModFit LT software (Verity Software House, version 5.0.9, Topsham, ME, USA). Singlet events were gated from the PI-area to PI-height plot before the cell cycle was analyzed. The results represent the mean of the data from two independent experiments.

SDS-PAGE & western blotting. The MV4-11 (5×10^5 cells per ml) or HeLa (7×10^4 cells per ml) cells were seeded in a Ø 100 mm Petri dish. The 24 h treatment began 4 h (MV4-11 cells) or 24 h (HeLa) after the seeding. After the treatment, the cells were harvested on ice, and pelleted (10 min, 1000 g, 4 °C) and resuspended in PBS (137 mM NaCl, 2.7 mM KCl, 1.5 mM KH_2PO_4, 6.4 mM Na_2HPO_4, pH 7.4) two times for the purpose of washing. Resulting pellet in a microtube was stored in the −80 °C freezer and later used for protein extraction by the RIPA buffer (20 mM Tris, 100 mM NaCl, 5 mM EDTA, 2 mM EGTA, 0.2% Nonidet P-40, 2 mM NaF, 1 mM PMSF, 1 mM Na_3VO_4, 2 μg mL^{-1} aprotinin, 0.5 μg mL^{-1} leupeptin) and using ultrasonic probe. The lysate was centrifuged (20 min, 14 000*g*, 4 °C), the supernatant was collected and its protein concentration was determined by the Bradford reagent. Samples were mixed with the 5× Laemmli buffer, denatured for 5 min at 98 °C and stored in the −80 °C freezer. Proteins (30 μg per well) in the samples were separated by SDS-PAGE according to the Laemmli method. Polyacrylamide gels composed of 4% stacking gel and 10% or 12.5% resolving gels were used for the separation in the Mini-PROTEAN electrophoresis system (Bio-Rad, USA). Proteins were then electroblotted (2 h, 270 mA) from the gel onto a nitrocellulose membrane (0.45 μm pore size) in the Mini *trans*-Blot system (Bio-Rad, USA). After transfer, the membrane was stained with 0.2% Ponceau S in 1% acetic acid. Dry membrane was cut into strips defined by the target protein to be detected and a molecular weight marker. Strips were destained in TBS (20 mM Tris, 150 mM NaCl, pH 7.6) and then blocked during incubation in 5% non-fat dry milk dissolved in TBS-T (20 mM Tris, 150 mM NaCl, 0.1% TWEEN 20, pH 7.6) for 1 h at the room temperature. Membranes were incubated with the primary antibodies in the milk solution overnight at 4 °C. Specific primary antibodies were used: anti-β-actin, anti-GAPDH (0411) (Santa Cruz Biotechnology, Santa Cruz, CA, USA); anti-caspase-7 (zymogen, fragment), anti-PARP (46D11), anti-Mcl-1 (D35A5), anti-HSP60 (D307), anti-cyclin B1 (V152), anti-histone H3 (D1H2) (all from Cell Signaling, Danvers, MA, USA); swine anti-rabbit HRP, rabbit anti-mouse HRP, anti-p-histone H3 (Ser10), anti-α-tubulin (DM1A), anti-Bcl-2 (Bcl-2-100) (all from Merck, Darmstadt, Germany); anti-β-tubulin (abcam, Cambridge, UK). Strips were washed in TBS and TBS-T and incubated with the HRP-conjugated secondary antibody for 1 h at room temperature. After the washings, strips were covered in SuperSignal West Pico chemiluminescent reagent (Thermo Fisher Scientific, USA) and the signal was recorded by the LAS-4000 camera (Fujifilm, Japan).

Tubulin polymerization assay by western blotting. HeLa cells were seeded into Petri dishes (Ø 100 mm), treated for 24 h and harvested by trypsinization. Cells were washed, resuspended in cold hypotonic buffer and incubated at 37 °C for 5 min as described by Wittmann *et al.*, after that, cells were centrifuged at 14 400*g* for 10 min at 4 °C.[48] Supernatants with soluble depolymerized tubulin fraction were collected. According to above-mentioned publication, pellets were lysed using modified RIPA buffers. Completely dissolved pellets were centrifuged at 14 400*g* at 4 °C for 10 min. Supernatants with polymerized tubulin fraction were collected. The amount of proteins in both fractions was determined by the Bradford reagent. Sample preparation, electrophoresis and western blotting were performed as described in section "SDS-PAGE & western blotting".

Tubulin polymerization assay. Direct time-dependent polymerization of tubulin protein was measured with a fluorescence based kit according to the manufacturer's procedure (Cytoskeleton, Inc., USA). The racemate and atropisomers were tested at the 100 μM concentration. The positive and negative controls (paclitaxel, colchicine) were used as recommended in the assay kit at the 3 μM concentration. We therefore maintain the ratio between effective concentrations of our compounds and positive/negative controls in cells and cell-free assay.

Caspase-3/7 activity assay. 24 h treated MV4-11 cells were harvested, lysed and quantified. The activity of caspase-3 and -7 was monitored by measuring the fluorescence of 7-amino-4-methylcoumarin (AMC) released from the fluorogenic peptide substrate Ac-DEVD-AMC. Aldehyde inhibitor Ac-DEVD-CHO of caspase-3 and-7 was used as a negative control. The method has been previously described in detail by Rárová *et al.*, 2016.[45]

Immunofluorescence microscopy. HeLa cells were seeded at a density of 6.0×10^4 cells per ml using 8-well ibidi slides (Munich, Germany). Cells were grown for 24 h and then treated with 10 nM or 3.75 μM racemates and isomers 5l and

5n, colchicine, myoseverin, nocodazole, paclitaxel (PTX), tubulysin or vincristine for 24 h. After the given time period of treatment, the cells were washed with PBS and fixed on the slides with cold acetone–methanol (1 : 1, v/v) for 10 min. The cells were subsequently labelled with primary antibody anti-α-tubulin (Merck, Darmstadt, Germany) overnight at 4 °C in the dark, washed with three changes of PBS, and incubated in appropriate fluorescently-conjugated secondary antibody (rabbit anti-mouse Alexa Fluor 488, Thermo, USA). The cells were then washed three times in PBS, in deionized water and mounted using the FluorSave (Merck, Darmstadt, Germany). Cells were visualized using a fluorescence microscope (IX51, Olympus, Japan) and compared with control untreated cells and positive controls.

Migration scratch assay. Confluent HUVECs were scratched and immediately treated with either full endothelial cell growth medium containing different substances or positive control (10 μM 2-methoxyestradiol). After 8 h of incubation, images were captured with a microscope (IX51, Olympus, Tokyo, Japan). Migration was calculated using in-house software and expressed as the ratio between pixels covered by cells and the total number of pixels in the wound area.[47]

Author contributions

J.P. performed almost the whole synthesis and wrote original draft together with T.H., P.C., L.R. and M.K. A.C. helped with synthesis. L.R., T.H., and M.K. – biological assay, formal analysis and visualization. I.N. – X-ray crystallography. O.K. developed chiral analytical and semi-preparative HPLC methods and separated compounds into individual atropisomers. P.C., L.R., and J.P. participated in writing – review & editing.

Data availability

The authors confirm that the data supporting the findings of this study are available within the article and its ESI† or upon request from the corresponding authors.

Conflicts of interest

There are no conflicts to declare.

Acknowledgements

Authors thank Anežka Šindlerová for excellent technical assistance and Adam Přibylka and Martin Grepl for chiral HPLC analyses of atropisomers. This work was supported by the Internal Grant Agency of Palacký University (IGA_PrF_2024_028). Biological testing was supported by grant from the Czech Science Foundation Nr. 23-05474S and the European Regional Development Fund – Project ENOCH (No. CZ.02.1.01/0.0/0.0/16_019/0000868).

References

1 L.-S. Feng, W.-Q. Su, J.-B. Cheng, T. Xiao, H.-Z. Li, D.-A. Chen and Z.-L. Zhang, *Arch. Pharm.*, 2022, **355**, 2200051.
2 H. A. Ibrahim and H. M. Refaat, *Future J. Pharm. Sci.*, 2020, **6**, 41.
3 S. Tahlan, S. Kumar, S. Kakkar and B. Narasimhan, *BMC Chem.*, 2019, **13**, 66.
4 D. Hernández-Romero, S. Rosete-Luna, A. López-Monteon, A. Chávez-Piña, N. Pérez-Hernández, J. Marroquín-Flores, A. Cruz-Navarro, G. Pesado-Gómez, D. Morales-Morales and R. Colorado-Peralta, *Coord. Chem. Rev.*, 2021, **439**, 213930.
5 A. de Dios, C. Shih, B. López de Uralde, C. Sánchez, M. del Prado, L. M. Martín Cabrejas, S. Pleite, J. Blanco-Urgoiti, M. J. Lorite, C. R. Nevill, R. Bonjouklian, J. York, M. Vieth, Y. Wang, N. Magnus, R. M. Campbell, B. D. Anderson, D. J. McCann, D. D. Giera, P. A. Lee, R. M. Schultz, L. C. Li, L. M. Johnson and J. A. Wolos, *J. Med. Chem.*, 2005, **48**, 2270–2273.
6 J.-C. Lien, C.-L. Chung, T.-F. Huang, T.-C. Chang, K.-C. Chen, G.-Y. Gao, M.-J. Hsu and S.-W. Huang, *Br. J. Pharmacol.*, 2019, **176**, 4034–4049.
7 Y. Ohno, R. Yi, A. Suganami, Y. Tamura, A. Matsumoto, S. Matsumoto, K. Saito and H. Shirasawa, *Anticancer Res.*, 2021, **41**, 699–706.
8 B. D. Palmer, J. B. Smaill, M. Boyd, D. H. Boschelli, A. M. Doherty, J. M. Hamby, S. S. Khatana, J. B. Kramer, A. J. Kraker, R. L. Panek, G. H. Lu, T. K. Dahring, R. T. Winters, H. D. H. Showalter and W. A. Denny, *J. Med. Chem.*, 1998, **41**, 5457–5465.
9 B. D. Palmer, A. J. Kraker, B. G. Hartl, A. D. Panopoulos, R. L. Panek, B. L. Batley, G. H. Lu, S. Trumpp-Kallmeyer, H. D. H. Showalter and W. A. Denny, *J. Med. Chem.*, 1999, **42**, 2373–2382.
10 R. G. Kulkarnia, S. A. Laufer, C. V. M. and A. Garlapati, *Med. Chem.*, 2013, **9**, 91–99.
11 E. M. E. Dokla, N. S. Abutaleb, S. N. Milik, D. Li, K. El-Baz, M.-A. W. Shalaby, R. Al-Karaki, M. Nasr, C. D. Klein, K. A. M. Abouzid and M. N. Seleem, *Eur. J. Med. Chem.*, 2020, **186**, 111850.
12 D. Secci, A. Bolasco, M. D'Ascenzio, F. Della Sala, M. Yáñez and S. Carradori, *J. Heterocycl. Chem.*, 2012, **49**, 1187–1195.
13 S. N. A. Bukhari, G. Lauro, I. Jantan, C. Fei Chee, M. W. Amjad, G. Bifulco, H. Sher, I. Abdullah and N. A. Rahman, *Future Med. Chem.*, 2016, **8**, 1953–1967.
14 S. R. Fletcher, E. McIver, S. Lewis, F. Burkamp, C. Leech, G. Mason, S. Boyce, D. Morrison, G. Richards, K. Sutton and A. B. Jones, *Bioorg. Med. Chem. Lett.*, 2016, **16**, 2872–2876.
15 Y.-L. Zhang, R. Yang, L.-Y. Xia, R.-J. Man, Y.-C. Chu, A.-Q. Jiang, Z.-C. Wang and H.-L. Zhu, *Bioorg. Chem.*, 2019, **92**, 103219.
16 Y. K. Yoon and T. S. Choon, *Arch. Pharm.*, 2016, **349**, 1–8.
17 F. Wang, X. Wang, M.-X. Zhang, Y.-H. Yang and H.-L. Zhu, *RSC Adv.*, 2015, **5**, 74425–74437.
18 Y. K. Yoon, M. A. Ali, A. C. Wei, A. N. Shirazi, K. Parang and T. S. Choon, *Eur. J. Med. Chem.*, 2014, **83**, 448–454.

19 M. M. Karpińska, J. Matysiak, A. Niewiadomy, J. Wietrzyk and D. Kłopotowska, *Monatsh. Chem. – Chem. Mon.*, 2012, **143**, 269–276.
20 S. R. LaPlante, P. J. Edwards, L. D. Fader, A. Jakalian and O. Hucke, *ChemMedChem*, 2011, **6**, 505–513.
21 M. Tomanová, I. Vaňková, D. Toman, A. Přibylka, I. Nemec and P. Cankař, *J. Org. Chem.*, 2023, **88**, 9265–9276.
22 M. Kriegelstein, D. Profous, A. Lyčka, Z. Trávníček, A. Přibylka, T. Volná, S. Benická and P. Cankař, *J. Org. Chem.*, 2019, **84**, 11911–11921.
23 M. Kriegelstein, D. Profous, A. Přibylka and P. Cankař, *J. Org. Chem.*, 2020, **85**, 12912–12921.
24 K. Janíková, L. Jedinák, T. Volná and P. Cankař, *Tetrahedron*, 2018, **74**, 606–617.
25 L. Jedinák, R. Zátopková, H. Zemánková, A. Šustková and P. Cankař, *J. Org. Chem.*, 2017, **82**, 157–169.
26 M. Pisár, E. Schütznerová, F. Hančík, I. Popa, Z. Trávníček and P. Cankař, *Molecules*, 2018, **23**, 149.
27 C. A. Belmokhtar, J. Hillion and E. Ségal-Bendirdjian, *Oncogene*, 2001, **20**, 3354–3362.
28 A. Kamal, A. B. Shaik, S. Polepalli, G. B. Kumar, V. S. Reddy, R. Mahesh, S. Garimella and N. Jain, *Bioorg. Med. Chem.*, 2015, **23**, 1082–1095.
29 F. Naaz, M. R. Haider, S. Shafi and M. S. Yar, *Eur. J. Med. Chem.*, 2019, **171**, 310–331.
30 S. A. Lakhani, A. Masud, K. Kuida, G. A. J. Porter, C. J. Booth, W. Z. Mehal, I. Inayat and R. A. Flavell, *Science*, 2006, **311**, 847–851.
31 S. Arora, X. I. Wang, S. M. Keenan, C. Andaya, Q. Zhang, Y. Peng and W. J. Welsh, *Cancer Res.*, 2009, **69**, 1910–1915.
32 E. Bausch, H. Kohlhof, S. Hamm, R. Krauss, R. Baumgartner and L. Sironi, *PLoS One*, 2013, **8**, e79594.
33 N. Mundhara, A. Majumder and D. Panda, *Sci. Rep.*, 2019, **9**, 7638.
34 A. Müller-Deku, J. C. M. Meiring, K. Loy, Y. Kraus, C. Heise, R. Bingham, K. I. Jansen, X. Qu, F. Bartolini, L. C. Kapitein, A. Akhmanova, J. Ahlfeld, D. Trauner and O. Thorn-Seshold, *Nat. Commun.*, 2020, **11**, 4640.
35 S. J. Nowak and V. G. Corces, *Trends Genet.*, 2004, **20**, 214–220.
36 Y. W. Chan, Y. Chen and R. Y. C. Poon, *Oncogene*, 2009, **28**, 170–183.
37 M. Castedo, J.-L. Perfettini, T. Roumier, K. Andreau, R. Medema and G. Kroemer, *Oncogene*, 2004, **23**, 2825–2837.
38 N. Sakurikar, J. M. Eichhorn and T. C. Chambers, *J. Biol. Chem.*, 2012, **287**, 39193–39204.
39 Y. H. Ling, C. Tornos and R. Perez-Soler, *J. Biol. Chem.*, 1998, **273**, 18984–18991.
40 I. B. Roninson, E. V. Broude and B. D. Chang, *Drug Resist. Update Rev.*, 2001, **4**, 303–313.
41 M. A. Jordan, K. Wendell, S. Gardiner, W. B. Derry, H. Copp and L. Wilson, *Cancer Res.*, 1996, **56**, 816–825.
42 M. A. Jordan, R. J. Toso, D. Thrower and L. Wilson, *Proc. Natl. Acad. Sci. U. S. A.*, 1993, **90**, 9552–9556.
43 Y. Y. Leung, L. L. Yao Hui and V. B. Kraus, *Semin. Arthritis Rheum.*, 2015, **45**, 341–350.
44 J. Zhou, D. Panda, J. W. Landen, L. Wilson and H. C. Joshi, *J. Biol. Chem.*, 2002, **277**, 17200–17208.
45 L. Rárová, J. Steigerová, M. Kvasnica, P. Bartůněk, K. Křížová, H. Chodounská, Z. Kolář, D. Sedlák, J. Oklestkova and M. Strnad, *J. Steroid Biochem. Mol. Biol.*, 2016, **159**, 154–169.
46 V. Malínková, E. Řezníčková, R. Jorda, T. Gucký and V. Kryštof, *Bioorg. Med. Chem.*, 2017, **25**, 6523–6535.
47 L. Rárová, D. Sedlák, J. Oklestkova, J. Steigerová, J. Liebl, S. Zahler, P. Bartůněk, Z. Kolář, L. Kohout, M. Kvasnica and M. Strnad, *J. Steroid Biochem. Mol. Biol.*, 2018, **178**, 263–271.
48 C. Wittmann, A. S. Sivchenko, F. Bacher, K. K. H. Tong, N. Guru, T. Wilson, J. Gonzales, H. Rauch, S. Kossatz, T. Reiner, M. V. Babak and V. B. Arion, *Inorg. Chem.*, 2022, **61**, 1456–1470.